The extension of the Periodic System: superheavy — superneutronic

W Greiner, V I Zagrebaev

Contents

Abstract. Nuclear reactions leading to formation of new superheavy elements and isotopes are discussed. The scope and limitations of different nuclear reactions (cold and hot synthesis, fusion of fission fragments, transfer reactions and reactions with radioactive ion beams) are analyzed, trying to find most promising reactions which may be used at available facilities. The bibliography includes 70 references.

I. Historical remarks

We begin our discussion of the Periodic Table with some historical remarks about Dmitri Medeleev and Julius Meyer, the discoverers of order and chemical systematics of the elements.

The two fathers of the Periodic System, Dmitri Ivanovich Mendeleev (27.1.1834 – 20.1.1907) and Julius Lothar Meyer (19.3.1830 – 11.4.1895) were contemporaries close in age. Although coming from different origins, they shared part of their education in science.

Meyer was virtually born into a scientific career. He came from a medical family of Oldenburg, Germany, and first pursued a medical degree. In medical school he became interested in chemistry, especially physiological topics like gases in the blood. He earned a medical doctorate at Würzburg university and subsequently also a physics

W Greiner Frankfurt Institute for Advanced Studies, J W Goethe University, Ruth-Moufang-Str. 1, 60438 Frankfurt am Main, Germany. Fax (49-069) 7984 7527, tel (49-069) 7984 7526, e-mail: greiner@fias.uni-frankfurt.de

V I Zagrebaev Flerov Laboratory of Nuclear Reaction of the Join Institute for Nuclear Research, ul. Joliot-Curie 6, 141980 Dubna, Moscow Region, Russia. Fax (7-496) 216 50 83, tel. (7-496) 216 47 62, e-mail: zagrebaev@jinr.ru

Ph.D. in Breslau (Wrozlaw). He then turned his focus to chemistry, becoming a professor in Karlsruhe (1868) and Tübingen (1876) where he remained for the rest of his career.

Mendeleev was born as the youngest of 17 children in Tobolsk, Siberia, where his father taught Russian literature and his mother operated a glassworks owned by the family. His mother — after her husband's death and shortly before her own — took the 15-year-old Dmitri to St Petersburg. There he attended the Main Pedagogical Institute and the University of St Petersburg, where he pursued a doctorate in chemistry. Immediately after his Ph.D. in 1865, he became professor at the St Petersburg Technological Institute and in 1867 at St Petersburg University. Mendeleev quickly rose to prominence, not only through his research in chemistry, but also because he became an advisor for industry and commerce. So he was guiding the development of the Russian petrol industry and also formulated the optimal conditions for distilling vodka. His sympathy for liberal causes frequently led him to protest against political oppression and bureaucracy and also caused him to resign his professorship in 1890. Nevertheless, he continued to play an important public role and was made director of the Russian Board of Weights and Measures, in which position he greatly contributed to the modernization of Russia.

During their graduate studies, Meyer and Mendeleev shared a common teacher, Robert Bunsen, with whom they worked at Heidelberg University a few years apart. Both Meyer and Mendeleev also were among the young scientists attending the first large international chemistry congress held at Karlsruhe in 1860, which did much to formulate and standardize the basic concepts of chemistry. Both were impressed with Stanislao Cannizzaro's presentation of Amedeo Avogadro s atomic hypothesis. Both Meyer and Mendeleev were driven to a systematic study of the known chemical elements by the need to teach chemistry courses. Since no up-to-date texts were available, they both decided to write textbooks of their own. For some time chemists had

been trying to devise a logical system of classification by arranging the elements by atomic weight, but confusion over how to determine atomic weights thwarted their attempts. Soon after Karlsruhe, various new atomic arrangements were published, culminating in the work of Meyer and Mendeleev.

In the first edition of 'Die modernen Theorien der Chemie' (1864), Meyer used atomic weights to arrange 28 elements into 6 families that bore similar chemical and physical characteristics, leaving a blank for an as-yet-undiscovered element. His main conceptual advance was to regard valence, the number that represents the combining power of an element, as the link among members of each family of elements and as the pattern for the order in which the families were themselves organized. The 28 elements were almost entirely main group elements. In 1868 Meyer also incorporated transition metals in a table which listed the elements in increasing weight order with elements with the same valence in a given column. Unfortunately for Meyer, however, this work was published only after the appearance of Mendeleev's first paper on the subject (1869).

After being appointed to the chair of chemistry at the University of St Petersburg, Mendeleev also had begun to write a textbook, 'Principles of Chemistry' (Osnovy Khimii, published between 1868 and 1870), and worked out the 'Periodic Law', which he first published in 1869. Mendeleev succeeded in arranging all known elements into one table. He also made precise predictions of the properties of not yet discovered elements, the most famous example being eka-silicon, or germanium, which was discovered only in 1886.

In 1870 Meyer published his classic paper 'Die Natur der chemischen Elemente als Function ihrer Atomgewichte', describing the evolution of his work since 1864. This paper is particularly famous for its graphic display of the perio-dicity of atomic volume plotted against atomic weight. This, as well as the subsequent correction of old atomic weights that the table cast in doubt helped to convert many chemists to the new ideas. Meanwhile, Meyer and Mendeleev carried on a long drawn-out priority dispute.

Even nearly one and a half century after its discovery, the Periodic System still is of current interest, because of the continuing discovery of new elements. The modern representation of the Periodic System will be given later in Section VIII.

II. Introduction

It is well known that the last element whose lifetime is comparable to the age of earth and that occurs in macro-scopic quantities in nature is uranium. All the other elements with $Z > 92$ have been produced in laboratory experiments (see historical review[1]). The progress in this field is quite impressive — 25 handmade new heavy elements have been synthesized within 60 years (Fig. 1). Some transuranium elements (up to californium) are produced in considerable quantity (by neutron capture process accompanied with β^- decay in nuclear reactors) sufficient to prepare a target that can be used for synthesis of the next SH elements in fusion reactions (see below).

Two significant pages in the synthesis of SH nuclei have been overturned within last twenty years. In the 'cold' fusion reactions based on the closed shell target nuclei, lead and bismuth, SH elements up to $Z = 113$ have been produced.[2-4] The 'world record' of 0.03 pb in production cross section of 113 element has been obtained here within
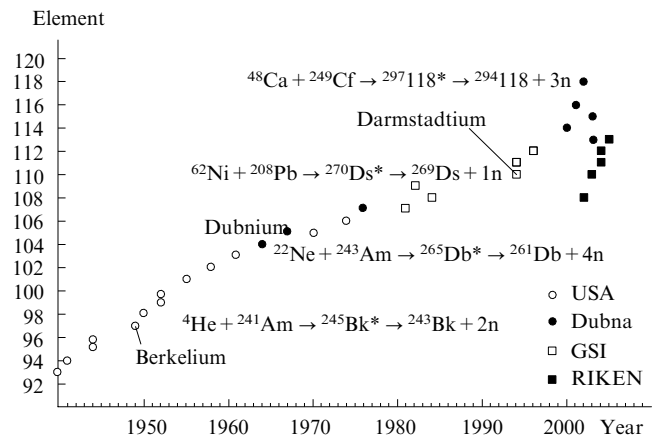

Figure 1. History of the laboratory production of heavy elements.

more than half-year irradiation of ^{209}Bi target with ^{70}Zn beam.[3,4] Further advance in this direction (with Ga or Ge beams) seems to be very difficult. Due to the 'curvature' of the stability line, in the 'cold' fusion reactions with stable nuclei we may produce only proton-rich isotopes of heavy elements situated along the proton drip line being very neutron-deficient with a short half-life (see Fig. 2), which is the main reason for the impossibility to reach the cenrte of the 'island of stability' ($Z \sim 114$, 120 and $N \sim 184$) in the superheavy mass region in fusion reactions with stable projectiles.
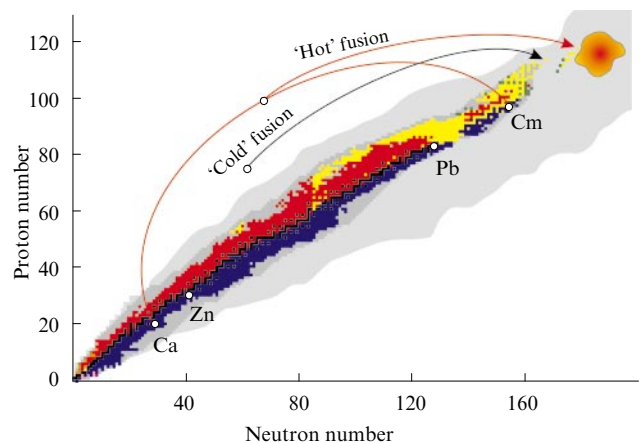

Figure 2. Superheavy nuclei produced in 'cold' and 'hot' fusion reactions.
Predicted island of stability is shown around $Z = 114$, 120 and $N = 184$. On Figs 2, 3, 29 and 30 stable nuclei are shown as black.

The cross sections for SH element production in more asymmetric (and 'hoter') fusion reactions of ^{48}Ca with actinide targets were found much larger.[5] Even 118 element was produced with the cross section of about 1 pb in the ^{48}Ca + ^{248}Cf fusion reaction.[6] Fusion of actinides with ^{48}Ca leads to more neutron-rich SH nuclei with much longer half-lives. Nevertheless, they are still far from the centre of the predicted 'island of stability' formed by the neutron shell around $N = 184$ (see Fig. 2). Note that these are the ^{48}Ca-induced fusion reactions which have confirmed the

existence of this 'island of stability'. In these reactions, a shore of the island was reached at last — the half-life of the $^{285}112$ isotope (produced in the 'hot' fusion reaction) is longer by almost five orders of magnitude as compared to the $^{277}112$ isotope of the same element produced in the 'cold' synthesis. Anyhow, californium is the heaviest actinide that can be used as a target material in this method (the half-life of the most long-living einsteinium isotope, $^{252}_{99}$Es, is 470 days, sufficient to be used as target material, but it is rather difficult to accumulate required amount of this matter).

As can be seen from Fig. 3, there is also a gap between the SH nuclei produced in the 'hot' fusion reactions with ^{48}Ca and the continent of known nuclei. This gap hinders one from obtaining a clear view of the properties of SH nuclei in this region. There are no combinations of stable nuclei to fill this gap in fusion reactions, and only the use of radioactive projectiles or transfer reactions (see below) may help one to do this.
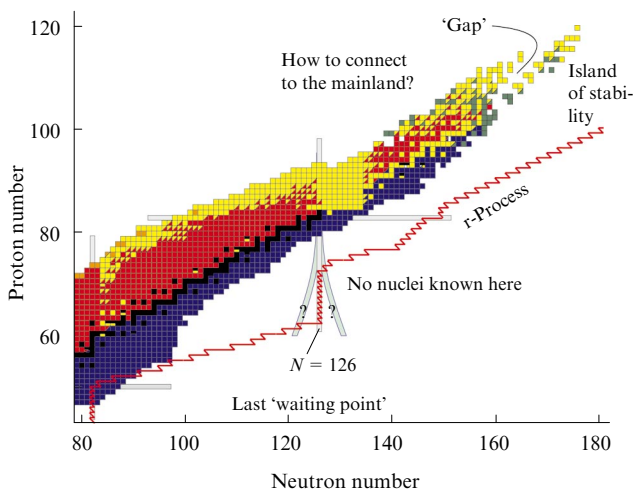

Figure 3. Top part of the nuclear map. The r-process path is shown schematically.

The other 'blank spot' is located at the 'north-east' of the nuclear map. The present limits of the upper part of the nuclear map is very close to stability while the unexplored area of heavy neutron-rich nuclides (to the east of the stability line) is extremely important for nuclear astrophysics investigations and, in particular, for the understanding of the r-process of astrophysical nucleo-genesis. According to a recent report by the National Research Council of the National Academy of Sciences (USA), the origin of heavy elements from iron to uranium remains one of the eleven greatest unanswered questions of modern physics (see, for example, Ref. 7) and it is likely to remain a hot research topic for the years to come. The r-process path is located (and interrupted by fission) just in the region of unknown heavy nuclei with a large neutron excess. The neutron shell $N = 126$ (and $Z \sim 70$) is the last 'waiting point' on this path (see Fig. 3). The half-lives and other characteristics of these nuclei are extremely important for the r-process scenario of the nucleosynthesis.[8] Study of the structural properties of nuclei along the neutron shell $N = 126$ could also contribute to the present discussion of the quenching of shell effects in nuclei with large neutron excess.

As a rule, new (neutron- and proton-rich) isotopes located far from the stability line are obtained in the fragmentation (spallation) processes at intermediate colliding energies, in fission of heavy nuclei and in low-energy fusion reactions. Two first methods are extensively used today for the production of new isotopes in the light and medium mass region including those which are close to the drip lines. For example, in the fragmentation of the ^{48}Ca beam with energy of about 140 MeV per nucleon the neutron-rich nuclides ^{44}Si, ^{42}Al and ^{40}Mg have been observed recently[9,10] with extremely low cross section of their production at the level of 1 pb. In this region of the nuclear map, the neutron drip line may stretch up to very exotic nuclei like ^{40}O (Ref. 11). However, the heavy neutron-rich nuclei located along the closed neutron shell $N = 126$ can be synthesized neither in fragmentation nor in fusion processes. Because of that, we also have almost no information about these nuclei — for example, there are 19 known neutron-rich isotopes of cesium ($Z = 55$) and only 4 of platinum ($Z = 78$).

In this connection it is clear that other ways for the production of SH elements with $Z > 118$, neutron-rich isotopes of SH nuclei in the region of the 'island of stability' and also those located at the 'north-east' part of the nuclear map should be searched for. In this paper we analyze abilities and limitations of different nuclear reactions leading to formation of SH elements ('cold' and 'hot' synthesis, symmetric fusion, transfer reactions and reactions with radioactive beams) trying to find most promising reactions that may be used at available facilities.[12]

A novel idea was recently proposed for the production of the heavy (and superheavy) neutron-rich nuclei *via* the multi-nucleon transfer processes of low-energy collisions of heavy ions.[13] It is well known that in the deep inelastic (damped) collisions of heavy ions the relative motion energy is quickly transformed into the internal excitation of the projectile-like and target-like reaction fragments, which are de-excited then by evaporation of light particles (mostly neutrons). This seems not to give us a chance for production of nuclei with large neutron excess in such reactions. However, if the colliding energy is rather low and the reaction Q-value is not very high, the formed primary reaction fragments might be not very much excited and will descend to their ground states after evaporation of a few neutrons thus remaining far from the stability line. The questions are how big is the cross section for the multi-nucleon transfer reactions at low colliding energies and could these reactions be considered as an alternative way for the production of exotic nuclei.

III. Shell structure of superheavy nuclei

Quantum effects leading to the shell structure of heavy nuclei play a crucial role in both stability of these nuclei and production of them in fusion reactions. The fission barriers of superheavy nuclei (preventing them from spontaneous fission and thus providing their existence) are determined completely by the shell structure. Studies of the shell structure of superheavy nuclei in the framework of the meson field theory and the Skyrme – Hartree – Fock approach show that the magic shells in the superheavy region are very isotopic dependent.[14] The forces with parameter set SkI4 predict both $Z = 114$ and $Z = 120$ as a magic numbers while the other sets predict only $Z = 120$. Estimated fission barriers for nuclei with $Z = 120$ are rather
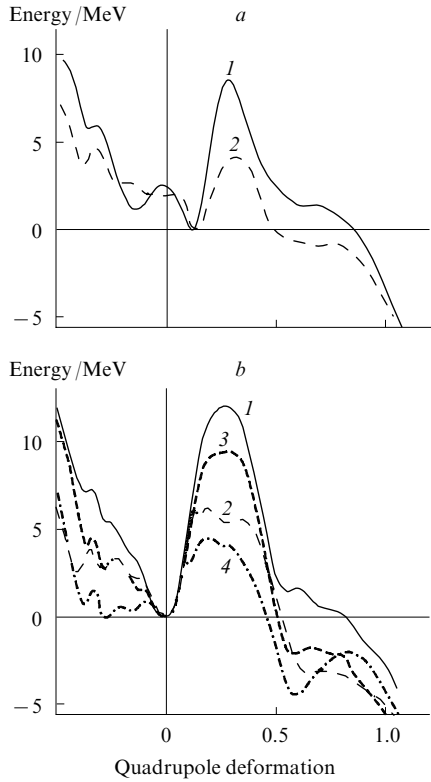
Figure 4. Fission barriers of superheavy nuclei $^{288}114$ (*a*) and $^{302}120$ (*b*) calculated within the relativistic mean field approach with different nucleon forces.[15]
(*1*) SLy6, (*2*) NL-Z2, (*3*) SkI3, (*4*) NL3.

high (see Fig. 4) though also depend strongly on a chosen set of the forces.[15]

The structure of superheavy nuclei might be rather unusual. Due to increasing role of the Coulomb repulsion, the calculated matter density distribution demonstrate more and more surface structure with increasing charge number (see Fig. 5). Hence these nuclei may get semi-bubble (or even alpha-clustering) density structure. It is clear that such structure reduces the Coulomb energy. This problem needs further investigation.
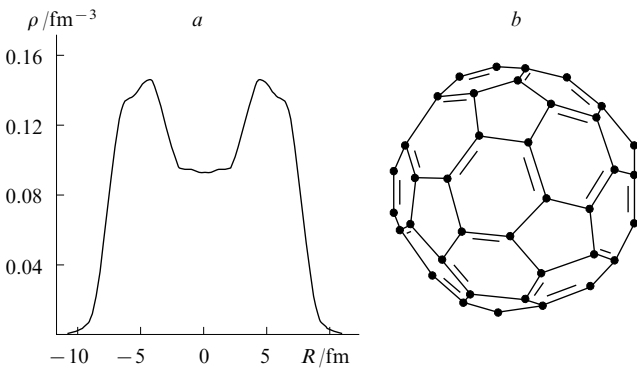

Figure 5. Matter density distribution (*a*) and a possibility for alpha-cluster (fullerene) structure of superheavy nucleus (*b*).
Nucleus $Z = 120$, $N = 180$, nucleon forces NL-Z2.

Shell effects play very important role also in low-energy collisions of heavy nuclei and, in particular, in fusion process. Interaction dynamics of two heavy nuclei at low (near-barrier) energies is determined mainly by the multi-dimensional adiabatic driving potential, which can be calculated within the two-centre shell model.[16] This potential energy surface demonstrates very pronounced shell structure by way of deep minima (ground and shape isomeric states) and valleys along which the heavy nuclear system predominantly moves in fusion, fission and quasi-fission (QF) processes.

An example of such driving potential is shown in Fig. 6 for the nuclear system consisting of 116 protons and 180 neutrons in the 'elongation – mass-asymmetry' space at
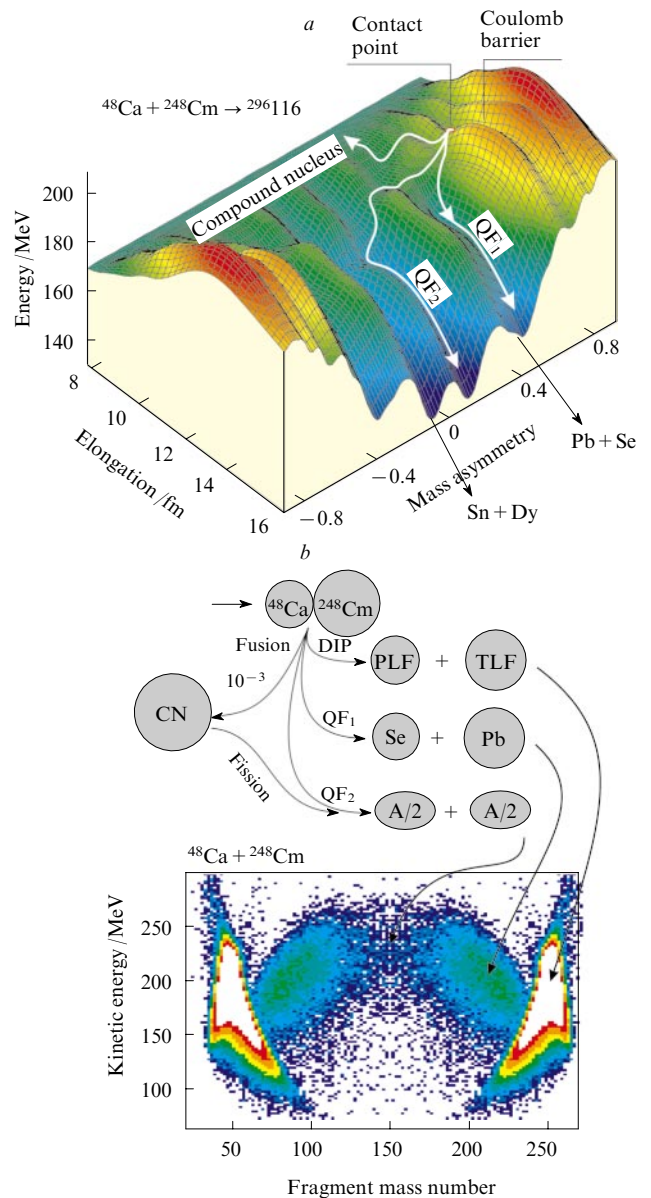

Figure 6. Three-dimensional view of the driving-potential for $^{48}Ca + ^{248}Cm$ at dynamic deformation $\beta_2 = 0.1$ (*a*).
The white curves with arrows show quasi-fission and fusion paths. At the bottom panel the experimental TKE-mass distribution [17] is shown with pronounced contributions of deep inelastic scattering ($A \approx 48.248$) and quasi-fission ($A \approx 98.208$) process (*b*).

fixed value of dynamic quadrupole deformation $\beta_2 = 0.1$. The shell effects become apparent in the deep valleys (cold valleys'), which are distinctly visible in the driving potential. They correspond to the formation of doubly magic nuclei in the exit channel: ^{208}Pb (at $\eta \approx 0.4$) and ^{132}Sn (at $\eta \approx 0.1$). After contact, the two heavy nuclei may re-separate with formation of projectile-like and target-like fragments (deep inelastic scattering). They may also form a mono-nucleus which evolves along the potential energy surface with significant nucleon rearrangement gradually sliding down to the valleys (quasi-fission process). Only in exceptional cases, due to fluctuations the heavy nuclear system may overcome all the barriers and form more or less spherical compound nucleus (fusion), which may then survive (emitting neutrons and gamma-rays) or fission (normal fission). Obtained by Itkis et al.[17] experimental data on the mass distribution of reaction fragments formed in low-energy collisions of heavy nuclei (bottom panel of Fig. 6) fully confirm such scenario.

The two-core shell effects remain important also for strongly overlapping nuclei leading to intermediate deep minima in the potential energy surface. These minima correspond to the shape isomeric states having a two-cluster character with magic or semimagic cores.[18]

IV. Superheavy element production in fusion reactions

The cross section of SH element production in heavy ion fusion reaction (with subsequent evaporation of x neutrons in the cooling process) is calculated as follows

$$\sigma_{ER}^{xn}(E) = \frac{\pi}{k^2} \sum_{l=0}^{\infty} (2l+1) P_{cont}(E,l) P_{CN}(E^*,l) P_{xn}(E^*,l), \quad (1)$$

where E is energy, $k = (2\mu E)^{1/2}/\hbar$ (μ is reduced mass of the system, $\hbar$ is Planck constant, l is the orbital momentum, $P_{cont}(E,l)$ is the penetrability of the multidimensional Coulomb barrier, $P_{CN}(E^*,l)$ is the probability of fusion of a heavy nucleus with the target nucleus, E^* is the excitation energy, $P_{xn}(E^*,l)$ is survival probability of an excited compound nucleus .

Empirical or quantum channel coupling models[19] may be used to calculate rather accurately penetrability of the multi-dimensional Coulomb barrier $P_{cont}(E,l)$ and the corresponding capture (sticking) cross section,

$$\sigma_{cap}(E) = \frac{\pi}{k^2} \sum (2l+1) P_{cont}$$

The survival probability $P_{xn}(E^*)$ of an excited compound nucleus (CN) can be calculated within a statistical model. We use here the fission barriers and other properties of SH nuclei predicted by the macro-microscopic model.[20] Other parameters determining the decay widths and the algorithm itself for a calculation of the light particle evaporation cascade and γ emission are taken from.[21] All the decay widths may be easily calculated also at the Web site.[19]

The probability for compound nucleus formation $P_{CN}(E,l)$ is the most difficult part of the calculation. The two-dimensional master equation was used for estimation of this quantity,[22] and a strong energy dependence of P_{CN} was found, which was confirmed recently in experiment.[23] Later the multi-dimensional Langevin-type dynamical equations were proposed[24,25] for the calculation of the

probability for CN formation in both 'cold' and 'hot' fusion reactions. The main idea is to study evolution of the heavy nuclear system driven by the time dependent multi-dimensional potential energy surface gradually transformed to the adiabatic potential calculated within the two-centre shell-model.[16] Note that the extended version of this model developed recently[26] leads to a correct asymptotic value of the potential energy of two separated nuclei and height of the Coulomb barrier in the entrance channel (fusion), and appropriate behaviour in the exit channel, giving the
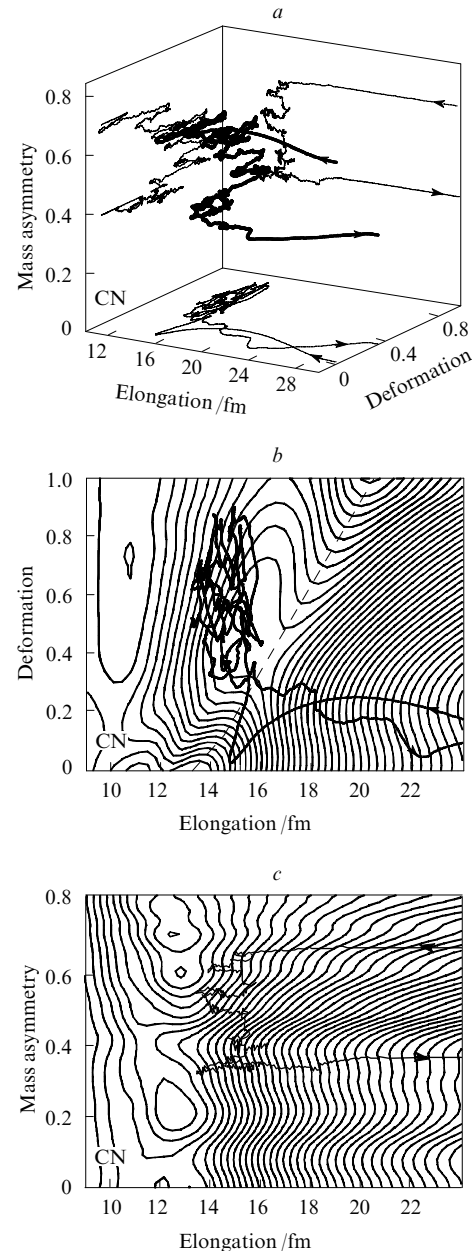

Figure 7. Collision of ^{48}Ca + ^{248}Cm at $E_{c.m.} = 210$ MeV. One of typical trajectories calculated within the Langevin equations and going to the quasi-fission exit channel (lead valley) is shown in the three-dimensional space (a) and projected onto the 'deformation–elongation' (b) and 'mass-asymmetry–elongation' (c) planes. The dashed line in (b) shows the ridge of the multi-dimensional Coulomb barrier.

required mass and energy distributions of reaction products and fission fragments.

In the case of near-barrier collision of heavy nuclei, only a few trajectories (of many thousands tested) reach the CN configuration (small values of elongation and deformation parameters, see Fig. 7). All others go out to the dominating deep inelastic and/or quasi-fission exit channels. One of such trajectories is shown in Fig. 7 in the three-dimensional space of 'elongation – deformation – mass-asymmetry' used in the calculations. The predictions for the excitation functions of SH element production with $Z = 112 - 118$ in $1n - 5n$ evaporation channels of the ^{48}Ca-induced fusion reactions [27, 28] made within our approach agree well with the experimental data obtained later. This gives us confidence in receiving rather reliable estimations of the reaction cross sections discussed below. Such estimations are urgently needed for planning future experiments in this field.

1. Cold fusion reactions

At near-barrier incident energies, fusion of heavy nuclei (^{48}Ca, ^{50}Ti, ^{54}Cr and so on) with ^{208}Pb or ^{209}Bi targets leads to formation of low-excited superheavy CN ('cold' synthesis). In spite of this favourable fact (only one or two neutrons are to be evaporated), the yield of evaporation residues sharply decreases with increasing charge of synthesized SH nucleus. There are two reasons for that. First, in these reactions neutron deficient SH nuclei are produced far from the closed shells or sub-shells. As a result, neutron separation energies of these nuclei are rather high whereas the fission barriers (macroscopic components plus shell corrections) are rather low (see Table 1). This leads to low survival probability even for 1n and 2n evaporation channels, Fig. 8.

Table 1. Fission barriers (B_{fis}) [macroscopical part (B_{LD}) and shell correction (S.C.)] and neutron separation energies (E_n^{sep}/MeV) of CN produced in the ^{48}Ca + ^{208}Pb, ^{50}Ti + ^{208}Pb and ^{54}Cr + ^{208}Pb fusion reactions.[20]

Compound nucleus	B_{LD}	S.C.	B_{fis}	E_n^{sep}	E_B^*
^{256}No	1.26	4.48	5.7	7.1	22
^{258}Rf	0.71	4.49	5.3	7.6	24
^{262}Sg	0.47	4.63	5.1	7.8	24

Note. The following notations are accepted here and in Table 2: B_{LD} is the macroscopical part of the fission barrier, S.C. is the shell correction, B_{fis} is the fission barrier, E_n^{sep} is the neutron separation energy. The last column shows the excitations of CN at the Bass barrier[29] incident energies.

The main reason for low yields of evaporation residues in these reactions is, however, a sharp decrease in the fusion probability with increasing charge of the projectile. In Fig. 9, the calculated capture, CN formation and evaporation residue (EvR) cross sections of the ^{208}Pb-induced fusion reactions are shown along with available experimental data on the yields of SH elements (not all experimental points are displayed to simplify the plot). The fusion probabilities P_{CN} calculated for head-on collisions (which bring the main contribution to the EvR cross sections) demonstrate a sharp energy dependence (see Fig. 10) found earlier.[22] Recently, the decrease in the fusion probability at subbarrier energies was confirmed experimentally for the fusion of ^{50}Ti with ^{208}Pb (Ref. 23).
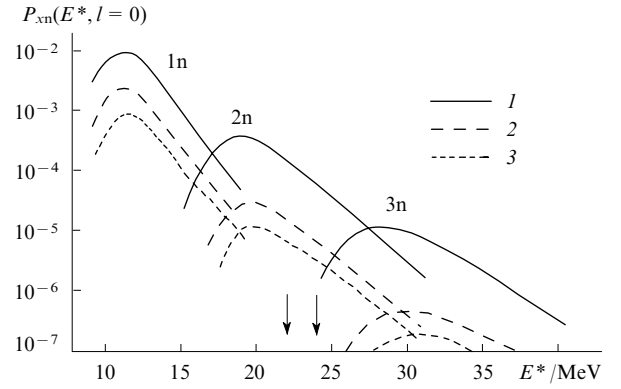

$P_{xn}(E^*, l = 0)$

Figure 8. Survival probability $P_{xn}(E^*, l = 0)$ of ^{256}No (*1*), ^{258}Rf (*2*) and ^{262}Sg (*3*) compound nuclei produced in the ^{48}Ca + ^{208}Pb, ^{50}Ti + ^{208}Pb and ^{54}Cr + ^{208}Pb fusion reactions.
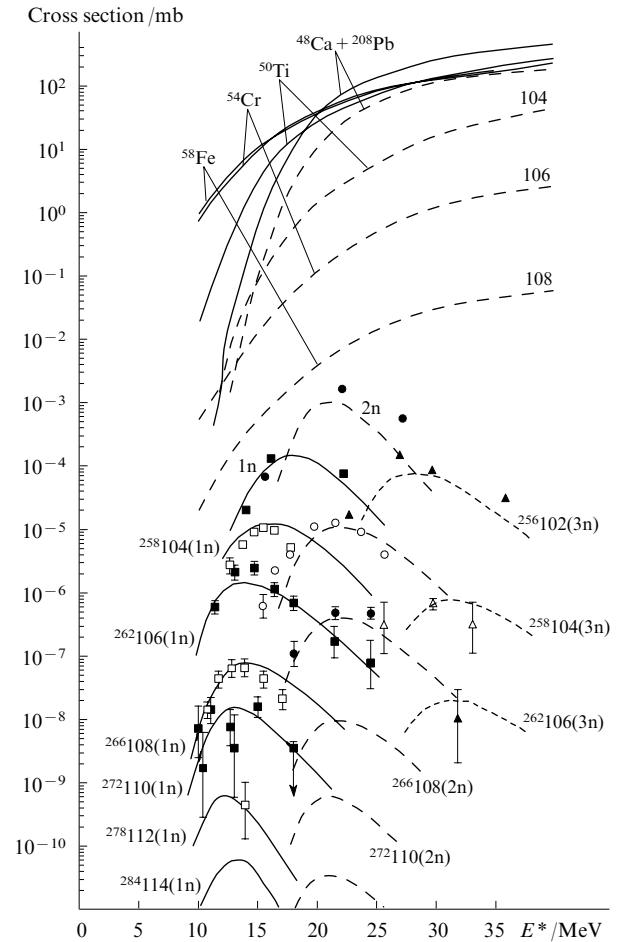The arrows indicate the Bass barriers (see Table 1).

Figure 9. Capture (upper solid curves), CN formation (short-dashed curves) and SH element production cross sections in the ^{208}Pb-induced fusion reactions.
1n, 2n and 3n evaporation channels are shown by solid, dashed and dotted curves (theory) and by rectangles, circles and triangles (experiment), correspondingly. Experimental data are taken from Refs 2–4 and 30.
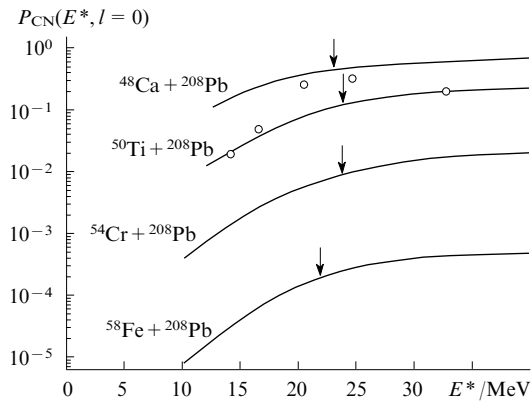
Figure 10. Calculated fusion probabilities, $P_{CN}(E^*, l = 0)$, for near-barrier collisions of heavy nuclei with ^{208}Pb target.
CN excitation energies at the Bass barriers are shown by the arrows. Experimental values of P_{CN} (Ref. 23) for the ^{50}Ti + ^{208}Pb fusion reaction are shown by the circles.
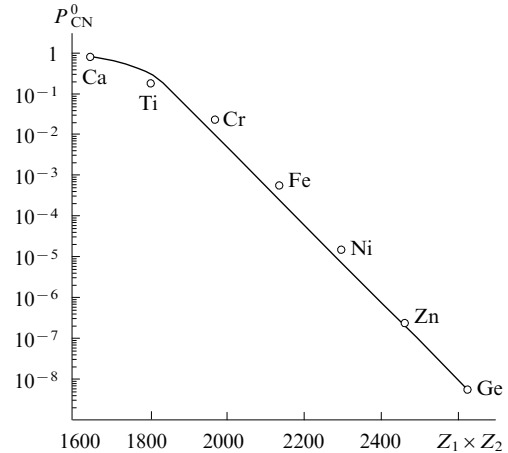

Figure 11. Above-barrier CN formation probability in the ^{208}Pb induced fusion reactions.
Results of calculation are shown by the circles, whereas the fitted curve corresponds to the expression (3).

We found that the calculated energy dependence of the fusion probability (shown in Fig. 10) may be approximated by the simple formula

$$P_{CN}(E^*, l) = P_{CN}^0 \left[1 + \exp\left(\frac{E_B^* - E_{int}^*(l)}{\Delta} \right) \right]^{-1}, \quad (2)$$

which could be useful for a fast estimation of EvR cross sections in the 'cold' fusion reactions. Here E_B^* is the excitation energy of CN at the center-of-mass beam energy equal to the Bass barrier.[29] E_B^* are shown in Fig. 10 by the arrows.

$$E_{int}^*(l) = E_{c.m.} + Q - E_{rot}(l)$$

is the 'internal' excitation energy which defines also the damping of the shell correction to the fission barrier of CN. Δ is the adjustable parameter of about 4 MeV, and P_{CN}^0 is the 'asymptotic' (above-barrier) fusion probability dependent only on a combination of colliding nuclei.

The values of P_{CN}^0 calculated at excitation energy $E^* = 40$ MeV (well above the barriers for the 'cold' fusion reactions) demonstrate rather simple behaviour (almost linear in the logarithmic scale) monotonically decreasing with an increase in charge of CN and/or the product of Z_1 and Z_2, see Fig. 11. This behaviour could also be approximated by very simple Fermi function

$$P_{CN}^0 = \left[1 + \exp\left(\frac{Z_1 Z_2 - \zeta}{\tau} \right) \right]^{-1}, \quad (3)$$

where $\zeta \approx 1760$ and $\tau \approx 45$ are just the fitted parameters. Eqn (3) is obviously valid only for the 'cold' fusion reactions of heavy nuclei with the closed shell targets ^{208}Pb and ^{209}Bi. Unfortunately, we have not enough experimental data to check this formula for other reactions (or to derive more general expression for the fusion probability).

Two important remarks could be done after our analysis of the 'cold' fusion reactions. The first is rather evident. There are no reasons (in fusion or in survival probabilities) to slow down the fast monotonic decrease in EvR cross sections with increasing charge of SH nucleus synthesized in the 'cold' fusion reaction. The yield of 114 element in the 1n evaporation channel of the ^{76}Ge + ^{208}Pb fusion reaction is

only 0.06 pb. For 116 and 118 elements synthesized in fusion reactions of ^{82}Se and ^{86}Kr with lead target, we found only 0.004 pb and 0.0005 pb, correspondingly, for 1n EvR cross sections. As already mentioned, fusion reactions with ^{20}Pb or ^{209}Bi targets lead to neutron-deficient SH nuclei with short half-lives, which may bring an additional difficulty to their experimental detection at the available separators.

The second conclusion is important for further experiments with actinide targets. The experimental value of EvR cross section for 104 element in the ^{50}Ti + ^{208}Pb fusion reaction is two orders of magnitude less as compared with the yield of 102 element in the ^{48}Ca + ^{208}Pb reaction (see Fig. 9). At first sight, this fact makes the fusion reactions of titanium with actinide targets ('hot' fusion) much less encouraging as compared to ^{48}Ca fusion reactions. However, this sharp decrease in the yield of the Rutherfordium isotopes is caused by the two reasons. One order of magnitude loss in the EvR cross section is due to the low survival probability of ^{258}Rf nucleus (the fission barrier is less by 0.4 MeV and neutron separation energy is higher by 0.5 MeV as compared with ^{256}No, Fig. 2), whereas fusion probability of ^{50}Ti with ^{208}Pb at energies near and above the Coulomb barrier is only one order of magnitude less than in the ^{48}Ca + ^{208}Pb fusion reaction (see Fig. 10). This makes titanium beam quite promising for synthesis of SH nuclei in fusion reactions with the actinide targets (see below).

2. Hot fusion reactions

Fusion reactions of ^{48}Ca with actinide targets lead to formation of more neutron-rich SH nuclei as compared to the 'cold' fusion reactions. Their half-lives are several orders of magnitude longer. For example, the half-life of the SH nucleus ^{277}112 synthesized in the 'cold' fusion reaction ^{70}Zn + ^{208}Pb is about 1 ms, whereas $T_{1/2}(^{285}112) \approx 34$ s (approaching the 'island of stability'). On average, these SH nuclei have higher fission barriers and lower neutron separation energies, which give them a chance to survive in the neutron evaporation cascade.

Unfortunately, weaker binding energies of the actinide nuclei lead to rather high excitation energies of obtained
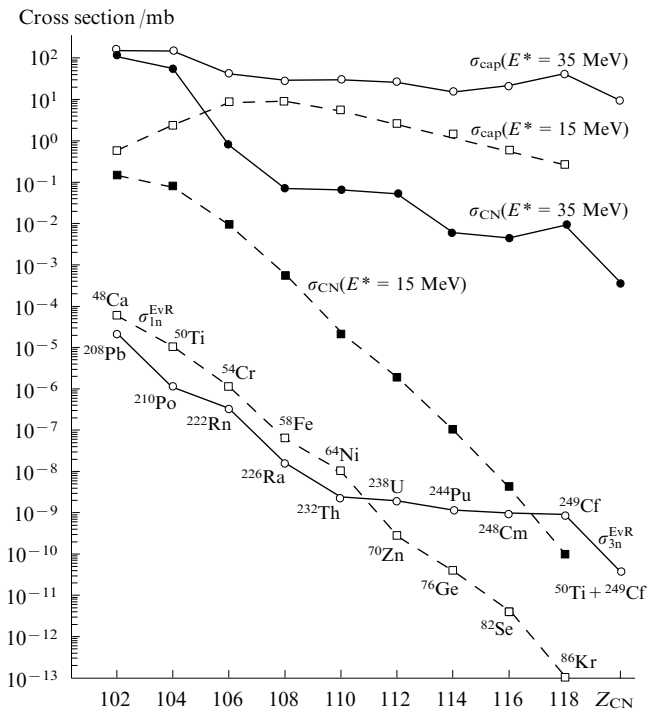
Cross section /mb

Figure 12. Calculated capture (σ_{cap}), fusion (σ_{CN}) and evaporation residue (σ^{EvR}) cross sections in the 'cold' ^{208}Pb induced (rectangles joined by dashed lines, projectiles are shown) and 'hot' ^{48}Ca induced (circles joined by solid lines, targets are shown) fusion reactions.
The cross sections are calculated at beam energies corresponding to 15 MeV ('cold' fusion, 1n channel) and 35 MeV ('hot' fusion, 3n channel) excitation energies of the compound nuclei.

CN (that is why these reactions are named 'hot'). At beam energy close to the Bass barrier, the value of

$$E^*_{\mathrm{CN}} = E_{\mathrm{c.m.}} + B(Z_{\mathrm{CN}}, A_{\mathrm{CN}}) - B(Z_1, A_1) - B(Z_2, A_2)$$

(B is the binding energy) is usually higher than 30 MeV for almost all the combinations, and at least 3 neutrons are to be evaporated to get a SH nucleus in its ground state. The total survival probability of CN formed in the 'hot' fusion reaction (in the 3n and/or in the 4n channel) is much less than 1n-survival probability in the 'cold' fusion reaction,

$$P^{\mathrm{hot}}_{3n}(E^* \approx 35\ \mathrm{MeV}) \ll P^{\mathrm{cold}}_{1n}(E^* \approx 15\ \mathrm{Mev}).$$

On the other hand, for the more asymmetric 'hot' combinations the fusion probability is usually much higher as compared to the 'cold' combinations leading to the same (but more neutron deficient) elements. We calculated the capture, fusion and EvR cross sections for the 'cold' (^{208}Pb-induced) and 'hot' (^{48}Ca-induced) reactions leading to SH nuclei with $Z = 102-118$ at the same excitation energies of the CN — 15 MeV for the 'cold' and 35 MeV for the 'hot' combinations. Of course, the beam energies, at which these CN excitations arise, are equal only approximately to the corresponding Coulomb barriers and not all of them agree precisely with positions of maxima of EvR cross sections. However, some general regularities can be found from these calculations.

The results of our calculations are shown in Fig. 12. As can be seen, the capture cross sections are about one order of magnitude larger for the 'hot' combinations. This is because the $E^* = 15$ MeV corresponds to the incident energies somewhat below the Bass barriers of the 'cold'
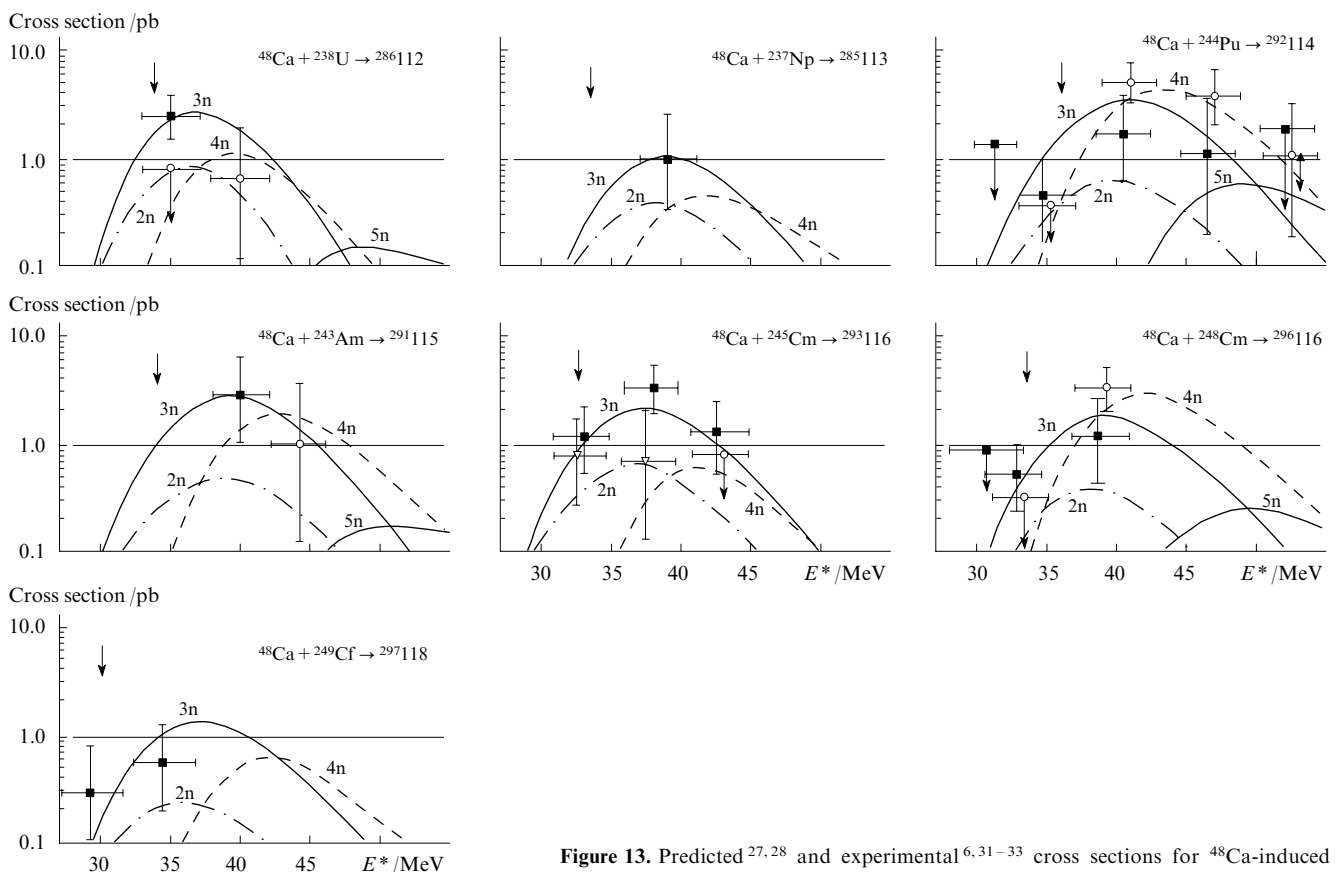

Figure 13. Predicted [27, 28] and experimental [6, 31–33] cross sections for ^{48}Ca-induced fusion reactions. The arrows indicate positions of the Bass barriers.

combinations. Slow decrease in σ_{cap} for the 'cold' combinations at $Z > 108$ is caused by gradual shallowing of the potential pocket (decreasing value of l_{crit}). Larger value of σ_{cap} for the $^{48}Ca + ^{249}Cf$ combination is conditioned by a 'colder' character of this reaction — the excitation energy of CN at the Bass barrier beam energy is only 28 MeV for this reaction (*i.e.*, $E^* = 35$ MeV corresponds here to above-barrier initial energy).

The fusion probability for the 'cold' combinations decreases very fast with increasing charge of the projectile and, in spite of evaporation of only one neutron, at $Z_{CN} \geqslant 112$ the EvR cross sections become less than in 'hot' fusion reactions. Increasing survival probability of SH nuclei with $Z = 114, 116$ synthesized in ^{49}Ca-induced fusion reactions as compared to $Z = 110, 112$ is due to the increase in the shell corrections to the fission barriers of these nuclei caused by approaching the closed shells predicted by the macro-microscopical model (see Table 2).

Table 2. Fission barriers (macroscopical part and shell correction) and neutron separation energies (MeV) of CN produced in the ^{48}Ca fusion reactions with ^{232}Th, $238U$, ^{244}Pu, ^{248}Cm and ^{249}Cf targets.[20] The last column shows the excitations of CN at the Bass barrier incident energies.

Compound nucleus	B_{LD}	S.C.	B_{fis}	E_n^{sep}	E_B^*
$^{280}110$	0.21	4.76	5.0	7.0	32
$^{286}112$	0.10	6.64	6.7	7.1	33
$^{292}114$	0.04	8.89	8.9	7.0	34
$^{296}116$	0.01	8.58	8.6	6.7	32
$^{297}118$	0.00	8.27	8.3	6.2	28

The experimental cross sections for synthesis of SH elements (from 112 to 118) in ^{48}Ca-induced fusion reactions well coincide with our predictions (performed before experiments). The corresponding excitation functions are shown in Fig. 13. The EvR cross sections reach maxima at energies well above the so-called Bass barriers[29] calculated for the corresponding spherical nuclei (see arrows in Fig. 13). That is because all the actinide target nuclei are well deformed and, as it was shown in Refs 25 and 27, the orientation effects play an important role in fusion reactions of statically deformed heavy nuclei. In contrast with the contact (capture) probability, the fusion probability (formation of CN) is strongly suppressed for more elongated 'nose-to-nose' initial orientations.[25] As a result, the preferable beam energies for synthesis of SH elements in the 'hot' fusion reactions are shifted to values which are several MeV higher than the corresponding Bass barriers (close to the fusion barriers for 'side-by-side' orientations).

In the series of SH elements synthesized in the ^{48}Ca-induced fusion reactions, one element, $Z = 117$, is still 'skipped'. The element 117 may be synthesized with rather large cross section in the $^{48}Ca + ^{249}Bk$ fusion reaction, if one manages to prepare a short-living (330 days) berkelium target. The calculated EvR cross sections of this reaction are shown in Fig. 14. It is important that the successive nuclei ($^{289,290}115$, $^{285,286}113$, $^{281,282}111$, $^{277,278}109$, and so on) appearing in the α-decay chains of $^{293,294}117$ are assumed to have rather long half-lives to be detected and studied in the chemical experiment, which makes the $^{48}Ca + ^{249}Bk$ fusion reaction quite attractive. Also the berkelium target may be used for synthesis of the element 119 in fusion reaction with the titanium beam (see below).
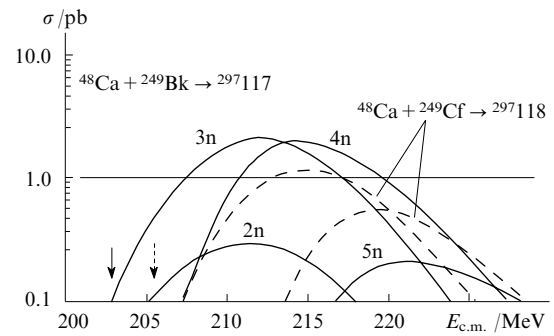

Figure 14. Cross sections for production of the element 117 in the $^{48}Ca + ^{249}Bk$ fusion reaction (solid curves, 2n, 3n, 4n and 5n evaporation channels). For comparison the EvR cross sections in 3n and 4n channels of the $^{48}Ca + ^{249}Cf$ fusion reaction are shown by the dashed curves.
The arrows indicate the corresponding Bass barriers.

As mentioned above, ^{249}Cf ($T_{1/2} = 351$ y) is the heaviest available target that may be used in the experiment. Thus, to get SH elements with $Z > 118$ in fusion reactions we
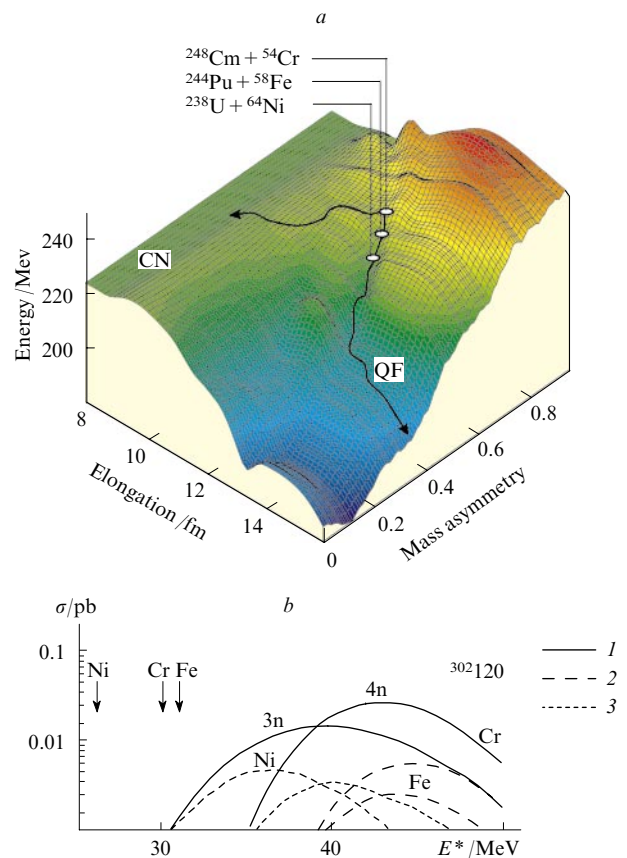

Figure 15. Potential energy surface for the nuclear system consisting of 120 protons and 182 neutrons (elongation – mass-asymmetry plot at fixed dynamic deformation $\beta_2 = 0.2$) (*a*).
Injection configurations (contact points) for the $^{54}Cr + ^{248}Cm$, $^{58}Fe + ^{244}Pu$ and $^{64}Ni + ^{238}U$ fusion reactions are shown by the circles. Thick curves with arrows shows schematically quasi-fission and fusion (CN formation) trajectories. At the bottom panel, the calculated excitation functions are shown for production of the $Z = 120$ element in 3n and 4n evaporation channels of the $^{54}Cr + ^{248}Cm$ (*1*), $^{58}Fe + ^{244}Pu$ (*2*) and $^{64}Ni + ^{238}U$ (*3*) fusion reactions. The corresponding Bass barriers are shown by the arrows (*b*).
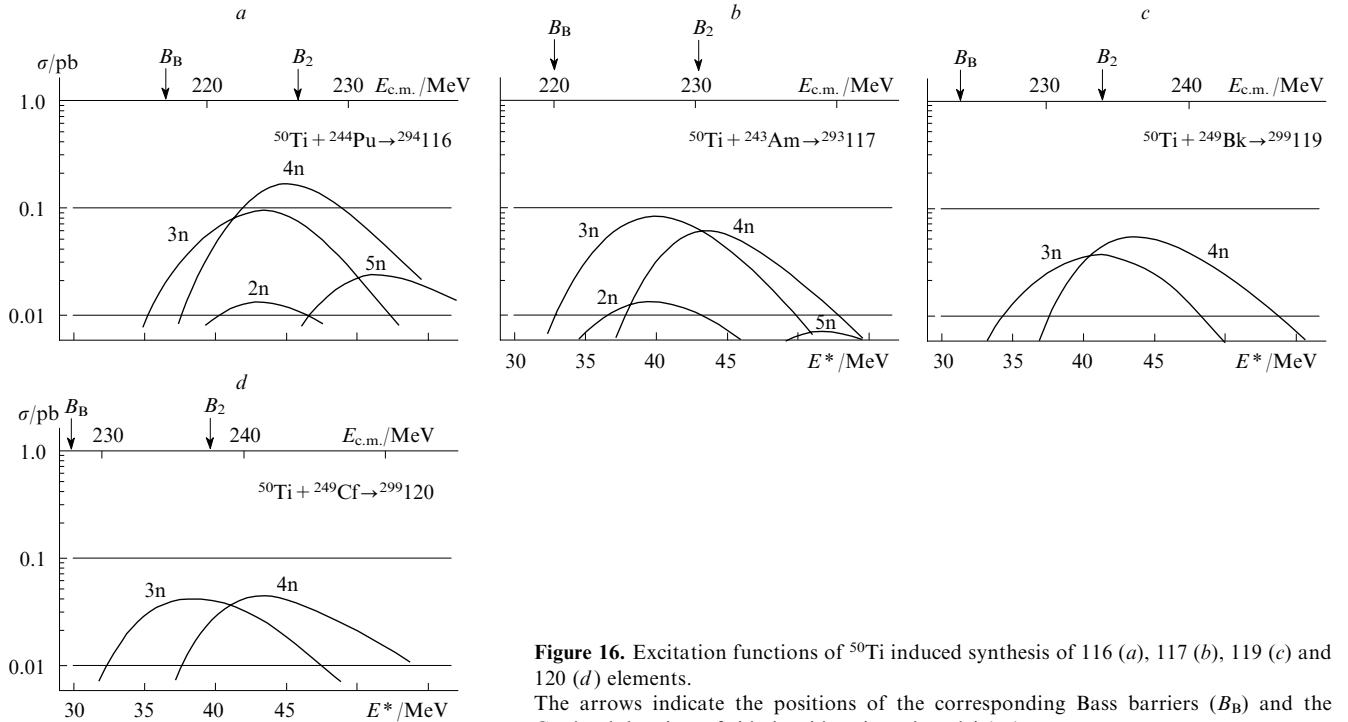
Figure 16. Excitation functions of ^{50}Ti induced synthesis of 116 (*a*), 117 (*b*), 119 (*c*) and 120 (*d*) elements.
The arrows indicate the positions of the corresponding Bass barriers (B_B) and the Coulomb barriers of side-by-side oriented nuclei (B_2).

should proceed to heavier than ^{48}Ca projectiles. Most neutron-rich isotopes of 120th element may be synthesized in the three different fusion reactions ^{54}Cr + ^{248}Cm, ^{58}Fe + ^{244}Pu and ^{64}Ni + ^{238}U leading to the same SH nucleus ^{302}120 with neutron number near to the predicted closed shell $N = 184$. These three combinations are not of equal worth. In Fig. 15, the potential energy surface for the nuclear system consisting of 120 protons and 182 neutrons is shown in the 'elongation – mass-asymmetry' space at fixed value of dynamic deformation $\beta_2 = 0.2$. One can see that the contact configuration of the more symmetric ^{64}Ni + ^{238}U combination is located lower in the valley leading the nuclear system to the dominating quasi-fission channels.

As a result, the estimated EvR cross sections for more symmetric ^{58}Fe + ^{244}Pu and ^{64}Ni + ^{238}U reactions are lower as compared to the less symmetric ^{54}Cr + ^{248}Cm combination (see Fig. 15). Some gain for ^{64}Ni + ^{238}U comes from the 'colder' character of this reaction — the excitation of CN at the Bass barrier incident energy for this combination, $E^*_{CN} = 26$ MeV, is much lower than for two others (see arrows in Fig. 15). Note that 3n and 4n evaporation residues of the ^{302}120 nucleus will decay over the known isotopes of 112 – 118 elements.[5] This significantly simplifies their identification. However, the Q-value of the first α-particle emitted from the element 120 should be rather high (about 13 MeV) and the half-life of this element might be rather short. If it is comparable with the time of flight of the recoil nucleus through a separator (about 1 μs), then an additional difficulty appears in detection of this element.

When calculating survival probability, we used the fission barriers of SH nuclei predicted by the macro-microscopical model,[20] which gives much lower fission barrier for ^{302}120 nucleus as compared to ^{296}116. On the other hand, the full microscopic models based on the self-consistent Hartree – Fock calculations [15] predict much higher fission barriers for the nucleus ^{302}120 (see Fig. 4) if the Skyrme forces are used (though these predictions are not unambig-

uous and depend strongly on chosen nucleon – nucleon forces). This means that the estimated 3n and 4n EvR cross sections in the fusion reactions considered above could be, in principle, a little bit higher than those shown in Fig. 15. This fact, however, influences neither the positions of the maxima of the excitation functions nor the conclusion about the advantage of the ^{54}Cr + ^{248}Cm fusion reaction as compared to ^{64}Ni + ^{238}U.

Strong dependence of the calculated EvR cross sections for the production of 120 element on mass-asymmetry in the entrance channel (along with their low values for all the reactions considered above) makes the nearest to ^{48}Ca projectile, ^{50}Ti, most promising for further synthesis of SH nuclei. Of course, the use of the titanium beam instead of ^{48}Ca also decreases the yield of SH nuclei mainly due to a worse fusion probability. The calculated excitation functions for synthesis of 116, 117, 119 and 120 SH elements in the fusion reactions of ^{50}Ti with ^{244}Pu, ^{243}Am, ^{249}Bk and ^{249}Cf targets are shown in Fig. 16. The maxima of the cross sections are located several MeV higher than the corresponding Bass barriers due to the orientation effects (see above). As can be seen from Fig. 16, the estimated EvR cross sections for 117, 119 and 120 SH elements synthesized in the ^{50}Ti-induced reactions are quite reachable at available experimental setups, though one needs longer time of irradiation as compared with ^{48}Ca fusion reactions.

V. Mass-symmetric fusion reactions

The use of the accelerated neutron-rich fission fragments is one of the widely discussed speculative methods for the production of SH elements in the region of the 'island of stability'. For example, in the ^{132}Sn + ^{176}Yb fusion reaction we may synthesize ^{308}120, which (after a few neutron evaporations and α-decays) may reach a centre of the 'island of stability'. Several projects in the world are now realizing to get the beams of neutron-rich fission fragments. The

question is how intensive should be such beams to produce SH nuclei. Evidently, the answer depends on the values of the corresponding cross sections. Unfortunately, there are almost no experimental data on fusion reactions in mass-symmetric nuclear combinations.

Experimental data on symmetric fusion reactions ^{100}Mo + ^{100}Mo, ^{100}Mo + ^{110}Pa and ^{110}Pa + ^{110}Pa show [34] that the fusion probability sharply decreases with increasing mass and charge of colliding nuclei. However, the last studied reactions of such kind, ^{110}Pa + ^{110}Pa, is still far from a combination leading to a SH compound nucleus. This means that further experimental study of such reactions is quite urgent.

The choice of the colliding nuclei is also important. In this connection the ^{136}Xe + ^{136}Xe fusion reaction looks very promising for experimental study,[35] because the formed CN, ^{272}Hs, should undergo just to symmetric fission. It means that two colliding ^{136}Xe nuclei are very close to the nascent fission fragments of ^{272}Hs in the region of the saddle point, and their fusion should really reflect a fusion process of two fission fragments.

The calculated within the two-center shell model adiabatic potential energy surface of the nuclear system consisting of 108 protons and 164 neutrons is shown in Fig. 17 as a function of elongation (distance between the centres) and deformation of the fragments at zero mass asymmetry, which correspond to two Xe nuclei in the entrance and exit channel. The energy scale is chosen in such a way that zero energy corresponds to two ^{136}Xe nuclei in their ground states at infinite distance. The contact configuration of two spherical Xe nuclei is located very close (in energy and in configuration space) to the saddle point of CN (note that it is located behind the Coulomb barrier, though there is no pronounced potential pocket). This fusion reaction is extremely 'cold', the excitation energy of the CN at the Bass barrier beam energy is only 5 MeV. One may expect that after contact these nuclei may overcome the inner barrier due to fluctuations of collective degrees of freedom
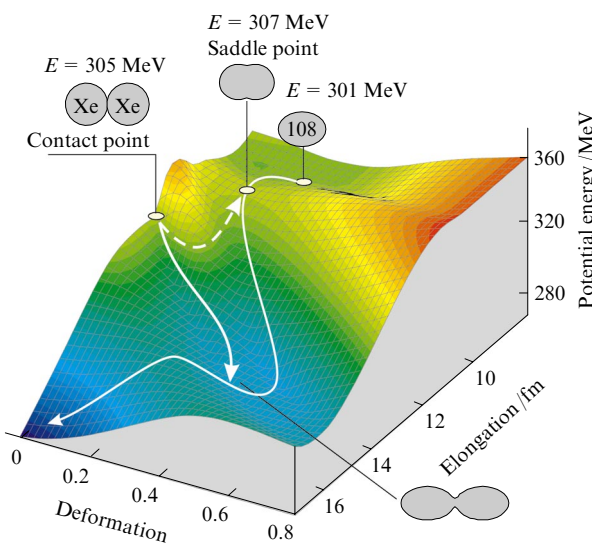
and thus reach the saddle configuration. After that they fuse (form CN) with 50% probability.

However, the potential energy decreases very fast with increasing deformations of the touching nuclei and drives the nuclear system to the fission valley (see Fig. 17). As a result, the calculated fusion probability is very low and, in spite of rather high fission barriers of the hassium isotopes in the region of $A \sim 270$ (~ 6 MeV [20]), the EvR cross sections were found to be very low,[36] (see Fig. 18). They are much less than the yield of ^{265}Hs synthesized in the more asymmetric ^{56}Fe + ^{208}Pb fusion reaction (Fig. 9). It is worthy to note that the prediction of the EvR cross section for the 1n channel in the ^{136}Xe + ^{136}Xe fusion reaction, obtained within the so-called 'fusion by diffusion' model,[37, 38] exceeds our result by three orders of magnitude. This fact reflects significant difficulties appearing in the calculation of the fusion probability in such reactions.
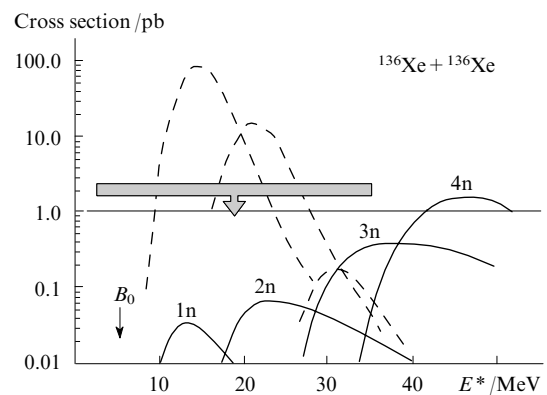
Figure 18. Evaporation residue cross sections in the ^{136}Xe + ^{136}Xe fusion reactions. Solid lines show our predictions,[36] whereas the dashed curves are the predictions of the 'fusion by diffusion' model.[38] Gray bar shows upper limit of the experimental EvR cross sections in this reaction.[39]

Experiment on the synthesis of hassium isotopes in the ^{136}Xe + ^{136}Xe fusion reaction was performed recently in Dubna, and no one event was detected at the level of about 2 pb.[39] Thus, we may conclude that for the widely discussed future experiments on synthesis of SH nuclei in the fusion reactions with accelerated fission fragments one needs to get a beam intensity not lower than 10^{13} pps (comparable or greater than intensities of available stable beams of heavy ions). Since the experimental values of the EvR cross sections in such reactions are still unknown, attempts to synthesize a SH element in the fusion reaction of two heavy more or less equal in masses nuclei (Xe + Xe or Sn + Xe) should be continued.

VI. Radioactive ion beams

Recently, many speculations have also appeared on the use of radioactive beams for synthesis and study of new elements and isotopes. As shown above, the use of accelerated fission fragments for the production of SH nuclei in symmetric fusion reactions is less encouraging and needs beam intensities at the hardly reachable level of 10^{13} pps or higher. In our opinion, they are the lighter radioactive beams which could be quite useful to solve the two important problems. As mentioned above, there is some gap

Figure 17. Adiabatic potential energy of the ^{272}108 nuclear system at zero mass asymmetry (^{136}Xe + ^{136}Xe configuration in asymptotic region) in the 'elongation – deformation' space. The curves with arrows show the fission and fusion paths. The circles show positions of CN, saddle point and contact configuration of two spherical Xe nuclei.

between the SH nuclei produced in the 'hot' fusion reactions with ^{48}Ca and the mainland. This gap hinders obtaining a clear view on the properties of SH nuclei in this region (in particular, positions of closed shells and sub-shells). There are no combinations of stable nuclei to fill this gap in fusion reactions, while the use of radioactive projectiles may help to do this.

The second problem that may be solved with the radioactive beams is obtaining much more neutron-rich transfermium isotopes. It is extremely important for two reasons. First, as we know from experiment, the addition of only 8 neutrons to nucleus ^{277}112 ($T_{1/2} = 0.7$ ms) increases its half-life by almost 5 orders of magnitude — $T_{1/2}(^{285}112) = 34$ s — testifying the approach of the 'island of stability'. How far is it? How long could be half-lives of SH nuclei at this island? To answer these questions we need to add more and more neutrons. Second, somewhere in the region of $Z \sim 100$ and $N \sim 170$ the r-process of nucleosynthesis should be terminated by neutron-induced or β-delayed fission. This region of nuclei, however, is absolutely unknown and only theoretical estimations of nuclear properties (rather unreliable for neutron-rich isotopes) are presently used in different astrophysical scenarios.

Contrary to a common opinion, neutron excess itself does not increase very much the EvR cross sections in fusion reactions of neutron rich radioactive nuclei. The neutron excess decreases just a little the height of the Coulomb barrier due to the small increase in the radius of neutron-rich projectile. Neutron transfer with positive Q-value may really increase the sub-barrier fusion probability by several orders of magnitude due to 'sequential fusion mechanism'.[40,41] However, this mechanism does not increase noticeably the fusion probability at near-barrier incident energies where the EvR cross sections are maximal (see above).

Shown in Fig. 19 are the EvR cross sections for the ^{44}S + ^{248}Cm fusion reaction in which the isotopes of the element 112 with six more neutrons (as compared with the ^{48}Ca + ^{238}U reaction) could be synthesized. The calculated one-picobarn cross sections mean that the beam intensity of sulfur-44 (which may be produced, for example, by 4p stripping from ^{48}Ca) should be no less than 10^{12} pps to synthesize these extremely neutron-rich isotopes.

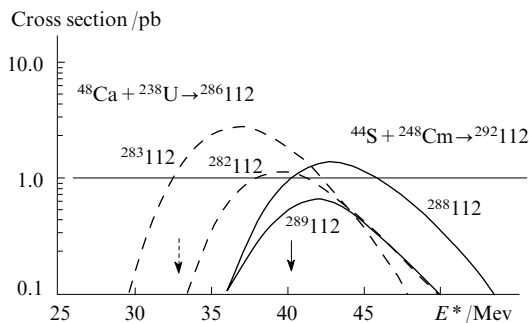In utmost mass-asymmetric fusion reactions (with lighter than neon projectiles) there is no suppression of
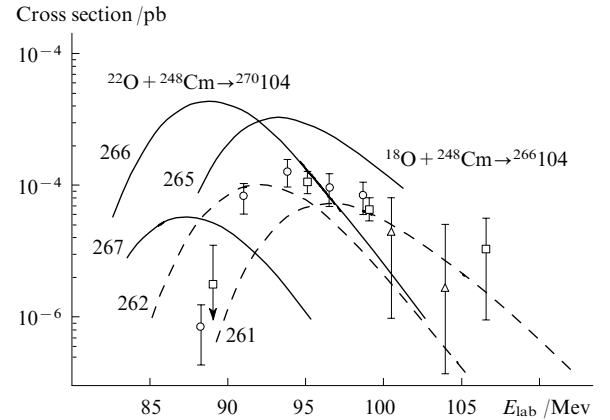
Figure 20. Excitation functions for synthesis of Rutherfordium isotopes in the ^{18}O + ^{248}Cm ($A = 261$ and $A = 262$, dashed curves) and ^{22}O + ^{248}Cm ($A = 265$, $A = 266$ and $A = 267$, solid curves) fusion reactions.
Experimental data for the ^{248}Cm(^{18}O,5n)^{261}Rf reaction are from Ref. 42 (rectangles), Ref. 43 (triangles) and Ref. 44 (circles).

CN formation: after contact colliding nuclei form CN with almost unity probability, $P_{CN} \approx 1$. This significantly increases the EvR cross sections in such reactions and, in spite of the rather difficult production of light radioactive nuclei with significant neutron excess, they could be used for the study of neutron-rich transfermium nuclei.

New heavy isotopes of Rutherfordium (up to ^{267}104) might be obtained in the ^{22}O + ^{248}Cm fusion reaction. The EvR cross sections in this reaction (shown in Fig. 20) are rather large and the beam intensity of ^{22}O at the level of 10^8 pps is sufficient to detect one decay event per week. Note that the reaction ^{22}O + ^{248}Cm is 3 MeV 'colder' as compared to ^{22}O + ^{248}Cm [E^*(Bass) = 41 and 44 MeV, respectively], which allows one to measure even the 3n evaporation channel leading to ^{267}104 (see Fig. 20). Half-lives of the heavy Rutherfordium isotopes ($A > 263$) should be rather long to use chemical methods for their identification.

VII. Multi-nucleon transfer reactions in damped collisions of heavy ions

Several models have been proposed and used for the description of mass transfer in deep inelastic heavy ion collisions, namely, the Focker–Planck[45] and master equations[46] for the corresponding distribution function, the Langevin equations,[47] and more sophisticated semiclassicall approaches.[48–50] We employ here the model of low-energy collisions of heavy ions.[24,25] This model is based on the Langevin-type dynamical equations of motion. The distance between the nuclear centres R (corresponding to the elongation of a mono-nucleus), dynamic spheroidal-type surface deformations β_1 and β_2, and mass asymmetry

$$\eta = \frac{A_2 - A_1}{A_1 + A_2}$$

are the most relevant degrees of freedom for the description of deep inelastic scattering and fusion-fission dynamics. To describe properly the yield of different isotopes of a given element (including extremely neutron rich ones) one needs

Figure 19. Excitation functions for the synthesis of the isotopes of the element 112 in 3n and 4n evaporation channels of the ^{48}Ca + ^{238}U ($A = 282$ and $A = 283$, dashed curves) and ^{44}S + ^{248}Cm ($A = 288$ and $A = 289$, solid curves) fusion reactions.
Arrows indicate the corresponding Bass barriers for the two reactions.

to consider separately neutron and proton transfers. Here we extend our model and (instead of only one mass-asymmetry variable) include into consideration the neutron and proton asymmetries,

$$\eta_N = \frac{2N - N_{CN}}{N_{CN}},$$

$$\eta_Z = \frac{2Z - Z_{CN}}{Z_{CN}}.$$

where N and Z are the neutron and proton numbers in one of the fragments, whereas N_{CN} and Z_{CN} refer to the compound nucleus. This noticeably complicates the problem because of the necessity to deal with the five-dimensional potential energy surface $V(R, \beta_1, \beta_2, \eta_N, \eta_Z)$. As before we restrict ourselves to the consideration of only one quadrupole dynamic deformation variable β instead of independent deformations β_1 and β_2 of two fragments. We assume 'equality of forces', i.e.,

$$C_1 \beta_1 = C_2 \beta_2,$$

where C_1 and C_2 are the LDM stiffness parameters of the fragments. Using this ratio and

$$\beta_1 + \beta_2 = 2\beta,$$

the deformations of the fragments are derived from the common variable β.

The potential energy is calculated within the double-folding procedure at initial (diabatic) reaction stage and within the extended version of the two-centre shell model [26] in the adiabatic reaction stage (see Fig. 21). Thus, for the nucleus-nucleus collisions at energies above the Coulomb barrier we use a time-dependent potential energy, which after contact gradually transforms from a diabatic potential energy into an adiabatic one:[24]

$$V(R, \beta, \eta_N, \eta_Z; t) = V_{diab}[1 - f(t)] + V_{adiab} f(t).$$

Here t is the time of interaction and $f(t)$ is a smoothing function satisfying the conditions $f(t = 0) = 0$ and $f(t \gg \tau_{relax}) = 1$, τ_{relax} is the adjustable parameter $\sim 10^{-21}$ s. Note that the diabatic, V_{diab}, and adiabatic, V_{adiab} potential energies depend on the same variables and
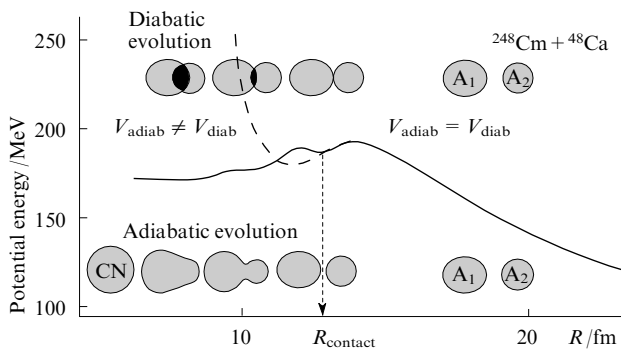

Figure 21. Potential energy of the nuclear system formed in fast (diabatic, dashed curve) and slow (adiabatic, solid curve) collision of ^{48}Ca with ^{248}Cm.

are equal to each other for well separated nuclei. Thus, the total potential energy, $V(R, \beta, \eta_N, \eta_Z; t)$, is a quite smooth function of t providing smooth driving forces $-\partial V / \partial q_i$.

For all the variables, with the exception of the neutron and proton asymmetries, we use the usual Langevin equations of motion with the inertia parameters, μ_R and μ_δ, calculated within the Werner – Wheeler approach.[51] For the mass and charge asymmetries, the inertialess Langevin type equations can be derived from the master equations for the corresponding distribution functions [24]

$$\frac{d\eta_N}{dt} = \frac{2}{N_{CN}} D_N^{(1)} + \frac{2}{N_{CN}} \sqrt{D_N^{(2)}} \Gamma_N(t), \qquad (4)$$

$$\frac{d\eta_Z}{dt} = \frac{2}{Z_{CN}} D_Z^{(1)} + \frac{2}{Z_{CN}} \sqrt{D_Z^{(2)}} \Gamma_Z(t),$$

where $\Gamma(t)$ is the normalized random variable with Gaussian distribution and $D^{(1)}$, $D^{(2)}$ are the transport coefficients.

Assuming that sequential nucleon transfers play a main role in mass rearrangement, i.e., $A' = A \pm 1$, we have

$$D_{N,Z}^{(1)} = \lambda_{N,Z}(A \to A + 1) - \lambda_{N,Z}(A \to A - 1), \qquad (5)$$

$$D_{N,Z}^{(2)} = \frac{1}{2}[\lambda_{N,Z}(A \to A + 1) + \lambda_{N,Z}(A \to A - 1)],$$

where the macroscopic transition probability $\lambda_{N,Z}^{(\pm)}(A \to A' = A \pm 1)$ is defined by the nuclear level density,[45, 46]

$$\lambda_{N,Z}^{(\pm)} = \lambda_{N,Z}^0 \left[\frac{\rho(A \pm 1)}{\rho(A)} \right]^{1/2},$$

and $\lambda_{N,Z}^0$ are the neutron and proton transfer rates. The nuclear level density

$$\rho \sim \exp(2\sqrt{aE^*})$$

depends on the excitation energy

$$E^* = E_{c.m.} - V(R, \delta_1, \delta_2, \eta_N, \eta_Z) - E_{rot}$$

and thus, on all the degrees of freedom used in the model. There is no information in the literature on a difference between neutron and proton transfer rates, and for simplicity we assume here that

$$\lambda_N^0 = \lambda_Z^0 = \frac{\lambda^0}{2},$$

where λ^0 is the nucleon transfer rate, which was estimated to be $\sim 10^{22}$ s^{-1} (Refs 45 and 46). We treat λ^0 as a parameter that should be chosen from the appropriate description of the available experimental data on mass transfer in deep inelastic scattering and quasi-fission.[24, 25]

For separated nuclei, the nucleon exchange is determined by extension of the tails of the single particle wave functions. This intermediate nucleon exchange plays an important role and has to be taken into account in Eqn (4). It can be treated by using the following final expression for the transition probability

$$\lambda_{N,Z}^{(\pm)} = \lambda_{N,Z}^0 \left[\frac{\rho(A \pm 1)}{\rho(A)} \right]^{1/2} P_{N,Z}^{tr}(R, \beta, A \to A \pm 1). \qquad (6)$$

Here $P_{N,Z}^{\text{tr}}(R, \beta, A \to A \pm 1)$ is the probability of one nucleon transfer, which depends on the distance between the nuclear surfaces and the nucleon separation energy. This probability goes exponentially to zero at $R \to \infty$ and it is equal to unity for overlapping nuclei. Here we used the semiclassical approximation for $P_{N,Z}^{\text{tr}}$ (Ref. 40). Equations (4)–(6) define a continuous change in charge and mass asymmetries in the whole space (obviously, $\mathrm{d}\eta_{N,Z}/\mathrm{d}t \to 0$ for far separated nuclei).

The double differential cross-sections of all the processes are calculated as follows

$$\frac{\mathrm{d}^2 \sigma_{N,Z}}{\mathrm{d}\Omega\,\mathrm{d}E}(E, \theta) = \int_0^\infty b\,\mathrm{d}b\,\frac{\Delta N_{N,Z}(b, E, \theta)}{N_{\text{tot}}(b)}\,\frac{1}{\sin(\theta)\Delta\theta\Delta E}. \quad (7)$$

Here $\Delta N_{N,Z}(b, E, \theta)$ is the number of events at a given impact parameter b in which a nucleus (N,Z) is formed with kinetic energy in the region $(E, E + \Delta E)$ and centre-of-mass outgoing angle in the region $(\theta, \theta + \Delta\theta)$, $N_{\text{tot}}(b)$ is the total number of simulated events for a given value of impact parameter. Expression (7) describes the mass, charge, energy and angular distributions of the primary fragments formed in the binary reaction. Subsequent de-excitation cascades of these fragments *via* emission of light particles and gamma-rays in competition with fission are taken into account explicitly for each event within the statistical model leading to the final distributions of the reaction products. The sharing of the excitation energy between the primary fragments is assumed to be proportional to their masses.

This model was successfully applied for description of the available experimental data on angular, energy and mass distributions of reaction products observed in the deep inelastic scattering of heavy ions at well above barrier energies [24, 25] and at centre-of-mass incident energies close to the Coulomb barrier.[52] Parameters of the model can be found in Ref. 25.

1. Production of SH elements in collisions of actinide nuclei

The use of multi-nucleon transfer from heavy-ion projectile to an actinide target nucleus for the production of new nuclear species in the transuranium region has a long history. Light (carbon,[53] oxygen and neon[54]), medium (calcium,[55, 56] krypton and xenon[57, 58]) and very heavy [^{238}U (Refs 59 and 60)] projectiles were used and heavy actinides (up to Mendelevium) have been produced in these reactions. The cross sections were found to decrease very rapidly with increasing transferred mass and atomic number of surviving target-like fragments. The level of 0.1 µb was reached for chemically separated Md isotopes.[60]

These experiments seem to give not so great chances for production of new SH nuclei. However, there are experimental evidences that the nuclear shell structure may strongly influence the nucleon flow in the low-energy damped collisions of heavy ions. For example, in ^{238}U-induced reactions on ^{110}Pd at about 6 MeV/u bombarding energy an enhanced proton flow along the neutron shells $N_1 = 82$ and $N_2 = 126$ (reached almost simultaneously in target-like and projectile-like fragments) was observed in the distribution of binary reaction products.[61] The idea to take advantage of the shell effects for the production of SH nuclei in the multi-nucleon transfer processes of low-energy heavy ion collisions was proposed.[62] The shell effects are known to play an important

role in fusion of heavy ions with actinide targets driving the nuclear system to the quasi-fission channels into the deep lead and tin valleys (see Fig. 6) and thus decreasing the fusion probability. On the contrary, in the transfer reactions the same effects may lead to enhanced yield of SH nuclei. It may occur if one of heavy colliding nuclei, say ^{238}U, gives away nucleons approaching to double magic ^{208}Pb nucleus, whereas another one, say ^{248}Cm, accepts these nucleons becoming superheavy in the exit channel — the so called 'inverse' (anti-symmetrizing) quasi-fission process.

The potential energy surface of the giant nuclear system formed in collision of ^{238}U and ^{248}Cm nuclei is shown in Fig. 22. It is calculated within the two-center shell model for a configuration of two touching nuclei (with fixed value of dynamic deformation $\beta_2 = 0.2$) depending on numbers of transferred protons and neutrons. The initial configuration of ^{238}U and ^{248}Cm touching nuclei is shown by the crosses.
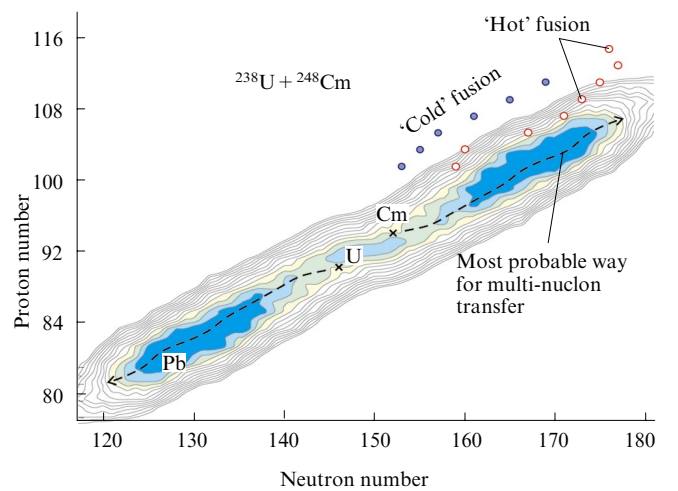

Figure 22. Landscape of potential energy surface of the nuclear system formed in collision of ^{238}U with ^{248}Cm (contact configuration, dynamic deformation $\beta_2 = 0.2$, contour lines are drawn over 1 MeV energy interval).
Open circles correspond to the most neutron-rich nuclei synthesized in ^{48}Ca induced fusion reactions while the filled ones show SH nuclei produced in the 'cold' fusion with lead target. The dotted line shows the most probable evolution in multi-nucleon transfer process.

In low-energy damped collisions of heavy ions just the potential energy surface regulates to a great extent the evolution of the nuclear system driving it to the minimal values of potential energy in the multidimensional space of collective variables. From Fig. 22 one sees that in the course of nucleon exchange the most probable path of the nuclear system formed by ^{238}U and ^{248}Cm lies along the line of stability with formation of SH nuclei that have many more neutrons as compared with those produced in the 'cold' and 'hot' fusion reactions. Due to fluctuations even more neutron-rich isotopes of SH nuclei may be formed in such transfer reactions.

The calculated cross sections for formation of primary fragments in low-energy collisions of ^{238}U with ^{248}Cm target are shown in Fig. 23 by the counter lines in logarithmic scale. As can be seen, the superheavy nuclei located very close to the centre of the island of stability may be produced
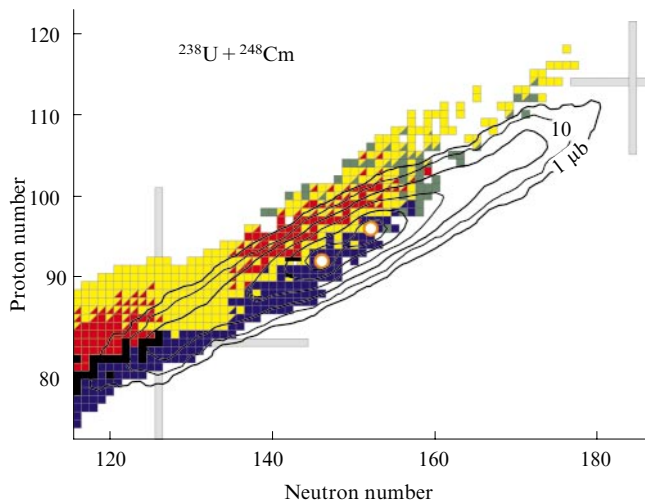
Figure 23. Landscape of the cross sections (microbarns, logarithmic scale) for production of primary fragments in collision of ^{238}U with ^{248}Cm at 800 MeV centre-of-mass energy (contour lines are drawn over one order of magnitude).

in this reaction with rather high cross section of one microbarn. Note one again that this region of the nuclear map cannot be reached in any fusion reaction with stable projectiles and long-lived targets. Of course, the question arises whether these excited superheavy primary fragments may survive in competition with fast fission, which is a dominated decay channel for them.

Really the yield of survived SH elements produced in the low-energy collisions of actinide nuclei is rather low, though the shell effects (see two double magic crossing in Fig. 23) give us a definite gain as compared to a monotonic exponential decrease in the cross sections with increasing number of transferred nucleons. In Fig. 24, the calculated EvR cross sections for production of SH nuclei in damped collisions of ^{238}U with ^{248}Cm at 800 MeV centre-of-mass energy are shown along with available experimental data. As can be seen, really much more neutron-rich isotopes of SH nuclei might be produced in such reactions [new isotopes of Siborgium ($Z = 106$) are shown in Fig. 24 by the open circles].

Certainly, the reliability of our predictions for the production of neutron-rich superheavy nuclei in the processes with transfer of several tens of nucleons is not very high. Up to now, very little experiments were performed on heavy-ion multi-nucleon transfer reactions at energies close to the Coulomb barrier and a role of the shell effects in these reactions is unknown. In this connection more detailed experiments have to be done aimed at the study of the shell effects in the mass transfer processes in low-energy damped collisions of heavy ions. The effect of 'inverse' quasi-fission may be studied also in experiments with less heavy nuclei. For example, in the collision of ^{160}Gd with ^{186}W we may expect an enhanced yield of the binary reaction products in the regions of Ba and Pb just due to the shell effect.[63] The experimental observation of this effect and the measurement of the corresponding enhancement factor in the yield of closed shell nuclei might allow us to make better predictions (and/or simple extrapolations) for heavier nuclear combinations, which are more difficult for experimental study.
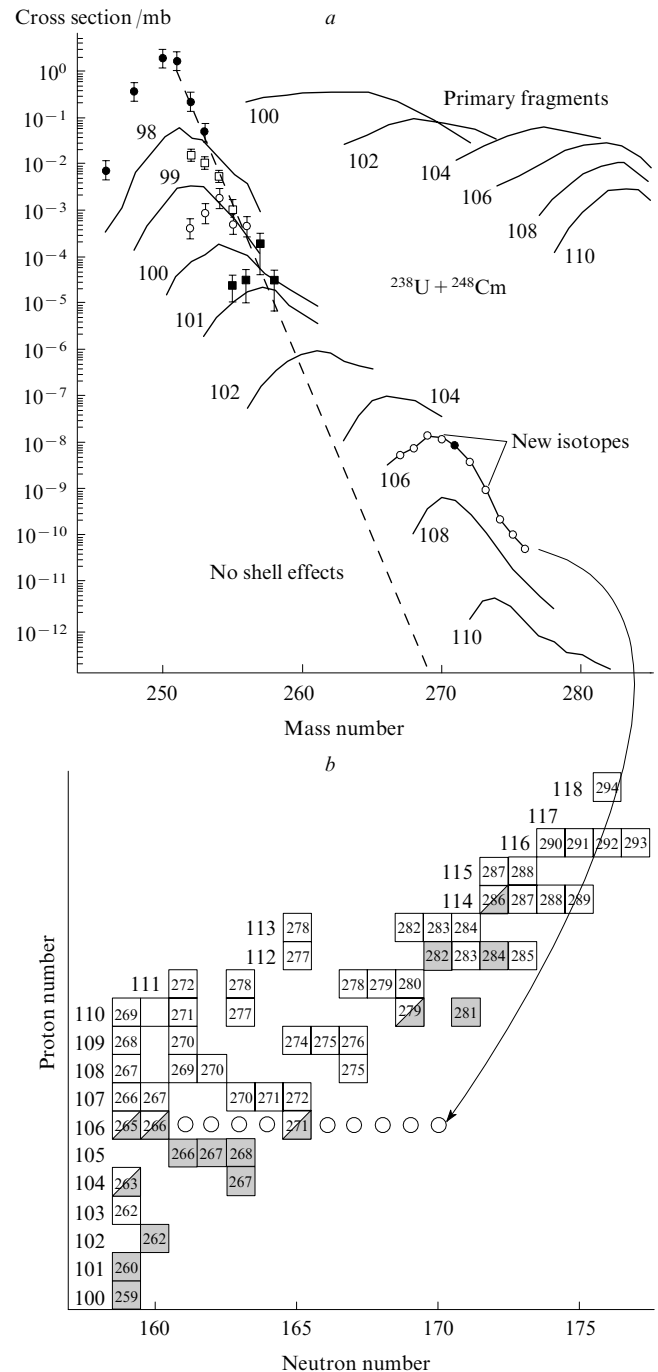

Figure 24. Yield of primary and survived isotopes of SH nuclei produced in collisions of ^{238}U with ^{248}Cm at 800 MeV centre-of-mass energy (*a*).
Experimental data[60] for Cf (filled circles), Es (open rectangles), Fm (open circles) and Md isotopes (filled rectangles) are also shown. Dashed line shows the expected locus of transfer reaction cross sections without the shell effects. Open circles at the curve with $Z = 106$ indicate unknown isotopes of Siborgium and their positions at the nuclear map (*b*).
Gray rectangles refer to nuclei with spontaneous fission.

2. Giant nuclear molecules and spontaneous positron formation

The time analysis of the damped collisions of actinide nuclei shows that in spite of non-existing attractive potential pocket the system consisting of two very heavy nuclei may
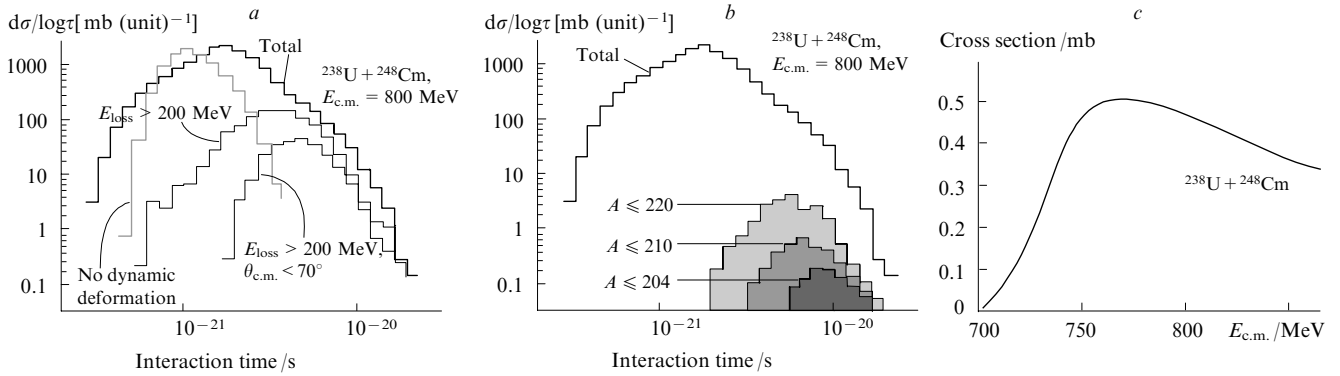
Figure 25. Reaction time distributions for the ^{238}U + ^{248}Cm collision at 800 MeV centre-of-mass energy. Thick solid histograms correspond to all events with energy loss more than 30 MeV.
(*a*) Dashed histogram shows the effect of switching-off dynamic deformations. Thin histograms show the reaction time distributions in the channels with formation of primary fragments with $E_{loss} > 200$ MeV and $E_{loss} > 200$ MeV, $\theta_{c.m.} < 70°$, correspondingly. (*b*) Shaded histograms show reaction time distributions in the channels with formation of primary fragments with $E_{loss} > 200$ MeV, $\theta_{c.m.} < 70°$ and $A \leqslant 220$, $A \leqslant 210$ and $A \leqslant 204$ (numbers near the histograms). (*c*) Cross section for events with interaction time longer than 10^{-20} s depending on beam energy.

hold in contact rather long in some cases. During this time, the giant nuclear system moves over the multidimensional potential energy surface with almost zero kinetic energy (the result of large nuclear viscosity). The total reaction time distribution, $d\sigma/\log\tau$ (τ denotes the time after the contact of two nuclei), is shown in Fig. 25 for the ^{238}U + ^{248}Cm collision. We found that the dynamic deformations are mainly responsible here for the time delay of the nucleus-nucleus collision. Ignoring the dynamic deformations in the equations of motion significantly decreases the reaction time, see Fig. 25 *a*. With increase in the energy loss and mass transfer, the reaction time becomes longer and its distribution becomes more narrow, see Fig. 25 *b*.

The lifetime of a giant composite system more than 10^{-20} s is quite enough to expect positron line structure emerging on top of the dynamical positron spectrum due to

spontaneous $e^+ e^-$ production from the supercritical electric fields as a fundamental QED process ('decay of the vacuum', see schematic Fig 26).[64, 65] The absolute cross section for long events $\tau \geqslant 10^{-20}$ s is found to be maximal just at the beam energy ensuring the two nuclei to be in contact, see Fig. 25 *c*. Note that the same energy is also optimal for the production of the most neutron-rich SH nuclei. Of course, there are some uncertainties in the used parameters, mostly in the value of nuclear viscosity. However we found only a linear dependence of the reaction time on the strength of nuclear viscosity, which means that the
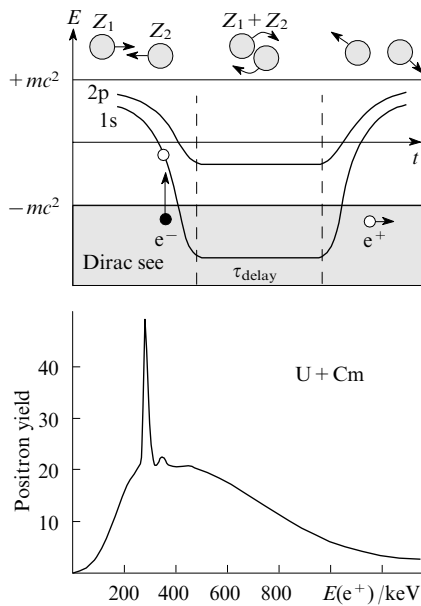

Figure 26. Spontaneous positron formation in supercritical electric field of long-lived giant quasi-atom.
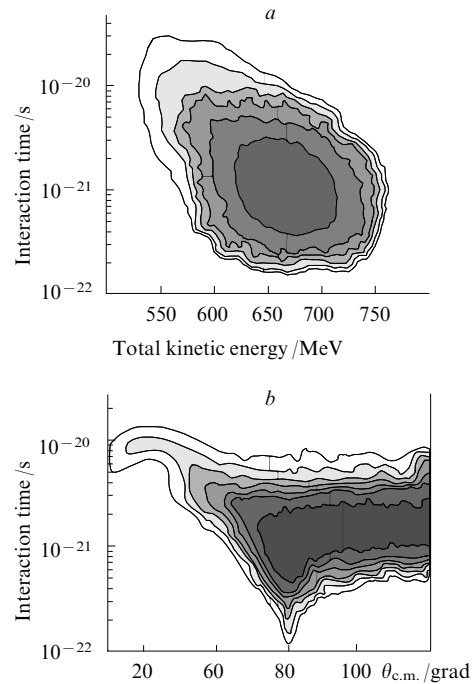

Figure 27. Energy–time (*a*) and angular–time (*b*) distributions of primary fragments in the ^{238}U + ^{248}Cm collision at 800 MeV ($E_{loss} > 15$ MeV).
Landscape is shown in logarithmic scale, lines are drawn over one order of magnitude. Quasi-elastic peak is removed.

obtained reaction time distribution is rather reliable, see logarithmic scale on both axes in Fig. 25 a. Note also that the time distribution shown in Fig. 5 corresponds to the time intervals between contact and scission of reaction fragments. However the electron eigenstates of the quasi-atom are weakly sensitive to a re-separation of nuclei (and depend on the total charge $Z_1 + Z_2$) as long as the distance between nuclear centers is shorter than the electron Compton wavelength (validating the monopole approximation for the Dirac orbits).[65, 66] Thus, the lifetime distribution of giant quasi-atoms is even slightly wider than it is shown in Fig. 25 a.

Formation of the background positrons in these reactions forces one to find some additional trigger for the longest events. Such long events correspond to the most damped collisions with formation of mostly excited primary fragments decaying by fission, see Figs 27 a. However there is also a chance for production of the primary fragments in the region of doubly magic nucleus ^{208}Pb, which could survive against fission due to nucleon evaporation. The number of the longest events depends weakly on impact parameter up to some critical value. On the other hand, in the angular distribution of all the excited primary fragments (strongly peaked at the centre-of-mass angle slightly larger than 90 °) there is the rapidly decreasing tail at small angles, see Fig. 27 b. Time distribution for the most damped events ($E_{loss} > 15$ MeV) in which large mass transfer occurs and primary fragments scatter in forward angles ($\theta_{c.m.}$) is rather narrow and really shifted to longer time delay, see hatched areas in Fig. 27 b.

For the considered case of ^{238}U + ^{248}Cm collision at 800 MeV centre-of-mass energy, the detection of the surviving nuclei in the lead region at the laboratory angles of about 25° and at the low-energy border of their spectrum (around 1000 MeV for Pb) could be a real trigger for longest reaction time.

3. Production of new heavy neutron-rich nuclei at the 'north-east' part of the nuclear map

Fusion reactions cannot be used also for the production of heavy neutron-rich nuclei at the 'north-east' part of the nuclear map especially those located along the closed neutron shell $N = 126$ (see Fig. 3). Properties of these nuclei are very important for astrophysical studies (probably this is the last 'waiting point' in the r-process of nucleosynthesis) and also for a possible distortion of shell effects in nuclei with an increase in neutron number.

One may assume that it is a neutron excess in the projectile that is most important for production of heavy neutron-rich nuclei. Therefore, we tested first the nucleon transfer probability in the near-barrier collision of neutron-rich nucleus ^{48}Ca with ^{208}Pb target. The calculated cross sections for the yield of target-like fragments (primary and coming to detector) are shown in Fig. 28. As can be seen, the cross sections for multi-nucleon transfer reactions are really rather high in this reaction. Nevertheless, in spite of the large neutron excess of the projectile, in the low energy collision of ^{48}Ca with ^{208}Pb we may produce only a few new neutron-rich nuclei at the level of one microbarn or less.

For the production of heavy neutron-rich nuclei located along the neutron closed shell $N = 126$ (probably it is the last waiting point in the r-process of nucleosynthesis), we propose to explore the multi-nucleon transfer reactions in low-energy collisions of ^{136}Xe with ^{208}Pb. The idea is to use the stabilizing effect of the closed neutron shells in both
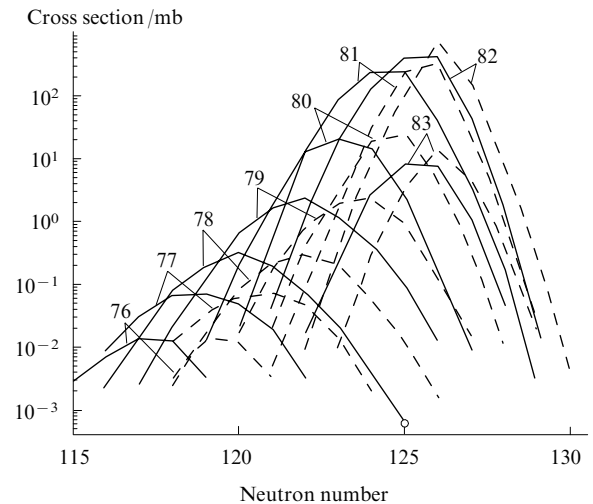

Figure 28. Cross sections for the production of target-like fragments in collisions of ^{48}Ca with ^{208}Pb at $E_{c.m.} = 185$ MeV.
The dashed curves show the yield of primary fragments and the solid ones correspond to survival nuclei. The open circle indicates unknown isotope of Pt.
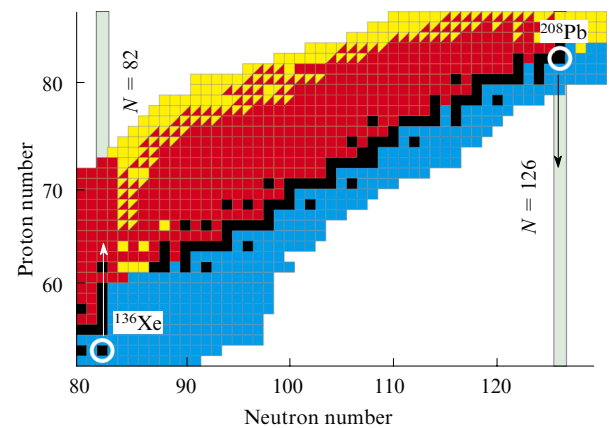

Figure 29. Schematic picture for proton transfer reactions in low-energy collisions of ^{136}Xe with ^{208}Pb.
Black rectangles indicate stable nuclei.

nuclei, $N = 82$ and $N = 126$, respectively (see Fig. 29). The proton transfer from lead to xenon might be rather favourable here because the light fragments formed in such a process are well bound (stable nuclei) and the reaction Q-values are almost zero, for example,

$$Q(^{136}\text{Xe} + {}^{208}\text{Pb} \longrightarrow {}^{142}\text{Nd} + {}^{202}\text{Os}) = -8.3 \text{ MeV}.$$
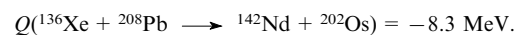
The landscape of the calculated cross sections for the yield of the different reaction fragments in low-energy collision of ^{136}Xe with ^{208}Pb is shown in the left panel of Fig. 30, whereas the cross sections for production of primary and survival heavy neutron-rich nuclei in this reaction at the energy $E_{c.m.} = 450$ MeV which is very close to the Coulomb barrier (the Bass barrier for this combination is about 434 MeV) is shown in the right panel of Fig. 31. Figure 32 demonstrates the yield of nuclei with closed neutron shell $N = 126$.
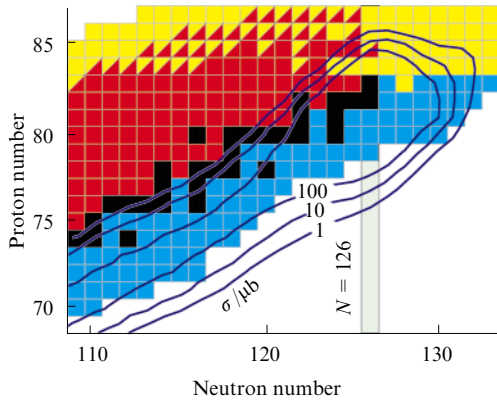
Figure 30. Landscape of the total cross section $d^2\sigma/dZdN$ (μb, numbers near the curves) for the production of heavy fragments in collisions of ^{136}Xe with ^{208}Pb at $E_{c.m.} = 450$ MeV. The contour lines are drawn over one order of magnitude.
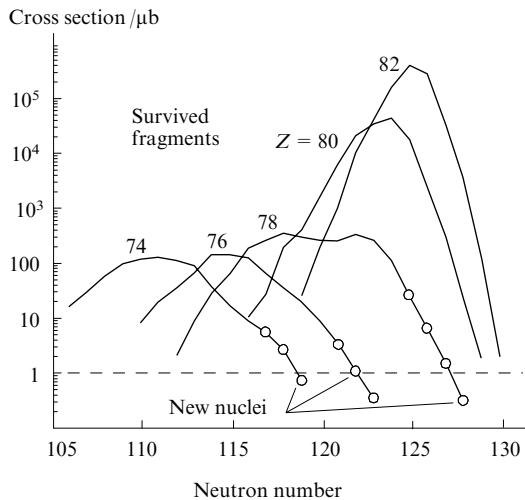

Figure 31. Cross sections for production of heavy neutron-rich nuclei in collisions of ^{136}Xe with ^{208}Pb at $E_{c.m.} = 450$ MeV. Open circles indicate unknown isotopes.
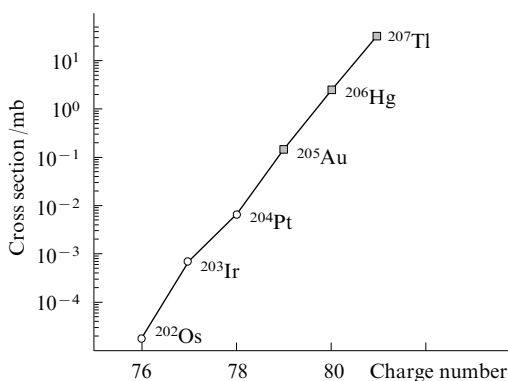

Figure 32. Yield of nuclei ^A_ZX$_{N=126}$ with neuron closed shell $N = 126$ in collisions of ^{136}Xe with ^{208}Pb at $E_{c.m.} = 450$ MeV.
Open circles indicate unknown isotopes.

Thus, our calculations demonstrate that the production of new heavy neutron-rich nuclei is quite possible in the multi-nucleon transfer processes of low-energy heavy ion collisions. As can be seen from Fig. 30, several tens of new nuclides in the region of $Z = 70 - 80$ can be produced with a cross section of 1 microbarn which is much higher than the level reached at available experimental setups. The production and study of unknown nuclei along the closed neutron shell $N = 126$ (see Fig. 32) is especially important because of the great interest in shell effects in heavy nuclei with large neutron excess. Note once again that these nuclei cannot be produced in fusion-fission and appear with extremely low probability in spallation of heavy nuclei at ultra-high beam energies.

VIII. The electronic structures of superheavy elements

The order of elements in the Periodic Table is determined by their electronic shell structures. For the then mostly hypothetical superheavy elements this was predicted rather early by Burkhard Fricke and Walter Greiner [67, 68] on the basis of relativistic Hartree – Fock calculations. Figure 33 [69] illustrates the results depicting the electronic shells in different colours. Let us briefly sum up the structure of the Periodic Table. In the first three periods of elements the 1s, the 2s and 2p, and the 3s and 3p shells are filled up sequentially, ending up with the chemically inert noble gases He, Ne, and Ar. In the next two periods, in addition, also the 3d and 4d shells are filled consecutively, giving rise to the transition metals. With growing atomic number, the energy differences between individual atomic levels become very small. In the 6th group, beginning with the element Lanthanum, the 4f and 5d shells are so close in energy that first a 5d electron is incorporated and than the 4f electrons follow. The situation becomes even more involved in the actinide region of the 7th group where two 6d electrons are first incorporated and then removed again in favour of the 5f electrons. The last actinide element, Lawrencium ($Z = 103$), contains all fourteen 5f electrons. Following that, the addition of the ten 6d and the six 7p electrons is expected, so that these elements should be similar to the elements Hafnium up to Radon in the sixth period. The element $Z = 114$ for which an increased stability is expected should be Lead-like. After that a new period (the eighth) begins, with alkali and alkaline earth elements at $Z = 119$ and $Z = 120$. The following shells 5g, 6f and 7d are energetically very close and will be filled concurrently. The situation is complicated by the fact that two of the six 8p electrons are specially favoured in energy and will be filled prematurely in this region. It is expected that the elements $Z = 122$ to $Z = 153$ will have no real analogues in the known region of the periodic system. Only for $Z = 154$ to $Z = 164$ will there be an analogy to the known d-elements. Unfortunately, the interesting chemistry of these 'superactinide' elements never will be known, because of the instability of the corresponding nuclei. The element $Z = 164$, which might be less unstable, is expected to be a chemically rather inert noble metal. It ends the eighth period and will be followed by the alkali and alkaline earth elements $Z = 165$ and $Z = 166$. Surprisingly, six p-elements are expected to follow, combining four electrons from the 8p and two from the 9p shell. The shell is closed at $Z = 172$ leading to a noble gas similar to Xenon.
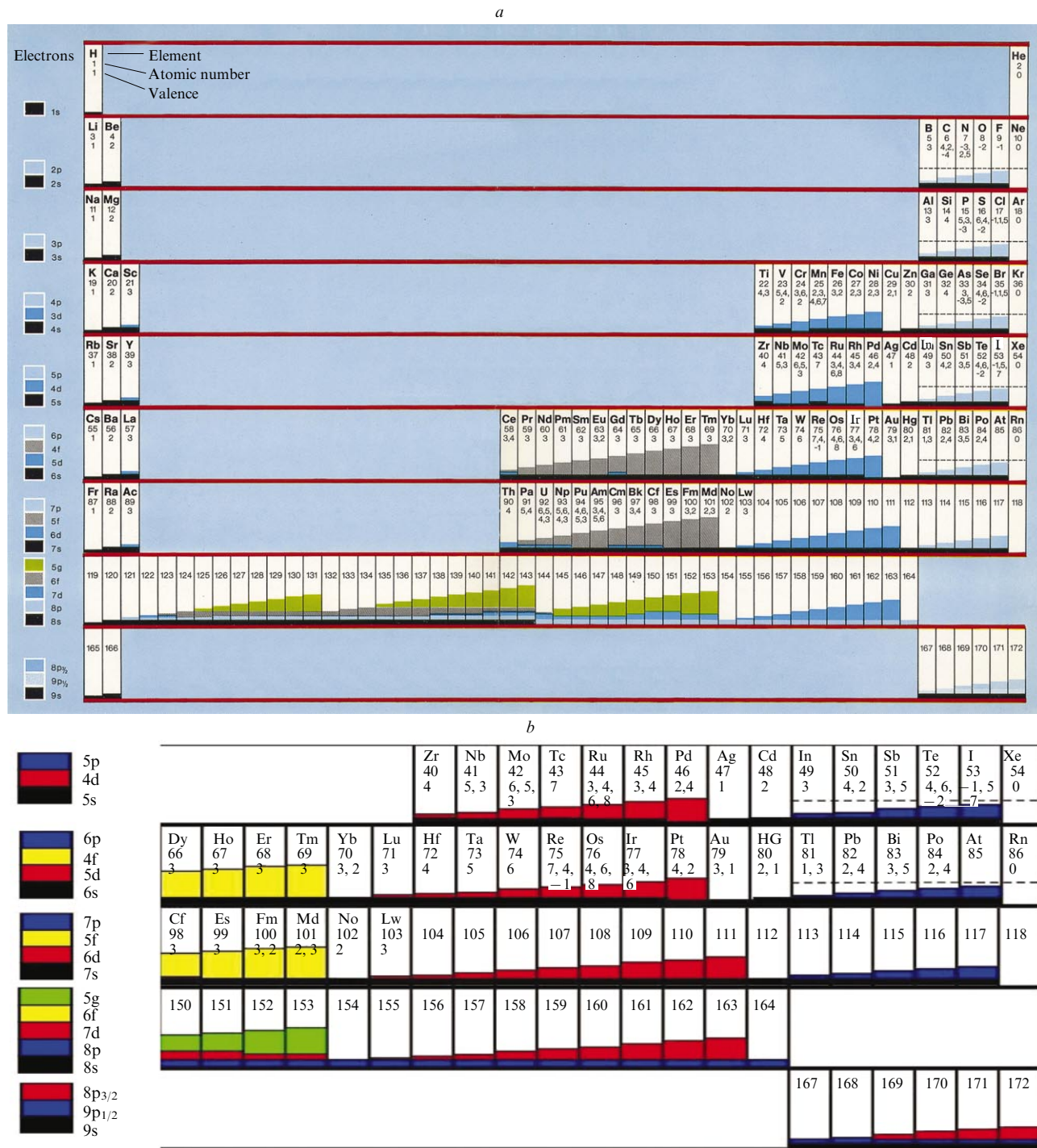
Figure 33. (*a*) The Periodic Table of elements extended into the region of superheavy nuclei, taken from Ref 69. (*b*) Detail of the above, depicting the experimentally accessible superheavy region.

Since these predictions have been made, about 40 years ago, tremendous experimental progress has been achieved in determining the chemical properties of superheavy elements. We refer in particular to the recent work by Robert Eichler, Sergey Dmitriev *et al*. at Dubna.[70] Having only a few atoms per element available, they investigated the chemistry of superheavy elements up to $Z = 114$ and confirmed the predictions by Fricke and Greiner. For example, the element 111 (*i.e.*, Roentgenium, Rg) is eka-gold and element 112 is eka-mercury. The situation for element 114,

predicted to be eka-lead, still is somewhat controversial. A reliable interpretation of the thermographic adsorption measurements[†] would need accurate calculations for the interaction of the superheavy atom with a multi-atomic substrate, which are not yet available.

† R Eichler, private communication, Dubna, 2009.

IX. Conclusion

Thus, we may conclude that there are several very promising possibilities for the synthesis of new SH elements and isotopes. First of all, we may use the titanium beam (instead of ^{48}Ca) and actinide targets to move forward up to the element 120. The estimated EvR cross sections are rather low (at the level of 0.1 pb) but quite reachable at available setups. If the experiments with titanium beam will confirm our expectations, then we have to find a possibility to increase the beam intensity and the detection efficiency (totally by one order of magnitude) and go on to the chromium and iron beams (aiming at the elements 122 and 124). The use of light and medium mass neutron-rich radioactive beams may help us to fill the gap between the new superheavy nuclei synthesized in ^{48}Ca-induced fusion reactions and the continent. Such a possibility is also provided by the multi-nucleon transfer processes in low-energy damped collisions of heavy actinide nuclei, if the shell effects really play an important role in such reactions. Parallel search for spontaneous positron emission from a supercritical electric field of long-living giant quasi-atoms formed in reactions with actinide nuclei is also quite promising. The production of SH elements in fusion reactions with accelerated fission fragments looks less encouraging. Only if an extremely high beam intensity will be attained, the promises are increasing.

We found a new method for synthesis of unknown heavy neutron-rich nuclei located in the 'north-east' part of the nuclear map. The properties of these nuclei are extremely important for the understanding the r-process of astrophysical nucleosynthesis of heavy elements. The study of the structural properties of nuclei along the neutron shell $N = 126$ would also contribute to the present discussion of the quenching of shell effects in nuclei with large neutron excess. This 'blank spot' of the nuclear map can be filled neither in fission reactions nor in fragmentation (or spallation) processes. Our calculations show that just the low-energy multi-nucleon transfer reactions can be used for the production of heavy neutron-rich nuclei. In particular, several tens of new isotopes of the elements with $Z = 70-80$ (also those located along the closed neutron shell $N = 126$) may be produced in the collision of ^{136}Xe with ^{208}Pb with cross sections higher than one microbarn. It is obvious that there are many other combinations of colliding nuclei. Uranium and thorium targets may be used, for example, for the production of new neutron rich isotopes with $Z \geqslant 82$. The use of accelerated neutron-rich fission fragments (which hardly may be useful for the synthesis of superheavy nuclei in fusion reactions due to low cross sections) looks especially promising for production of new heavy isotopes in low-energy multi-nucleon transfer processes.

Cross sections of one microbarn are quite reachable at the available experimental setups. However, the identification of new heavy nuclei obtained in the multi-nucleon transfer reactions is a rather complicated problem. Most of these nuclei undergo β^--decay. The atomic mass could be determined by the time-of-flight technique rather accurately. The identification of the atomic number of the heavy nucleus is more difficult. The same is true for the determination of its half-life, which is the most important property of the nuclei in the region of $N \sim 126$ (last waiting point in the r-process). In principle, it could be done by the registration of the electron cascade in the β^--decay chain (coming from the same position) in coincidence with the gamma-rays of the daughter nuclei. Anyhow, the synthesis and study of these nuclei (important for many reasons) is a challenge for low-energy nuclear physics now and in forthcoming years.

References

1. G T Seaborg, W D Loveland *The Elements Beyond Uranium* (New York: Wiley, 1990)
2. S Hofmann, G Münzenberg *Rev. Mod. Phys.* **72** 733 (2000)
3. K Morita, K Morimoto, D Kaji, T Akiyama, S Goto, H Haba, E Ideguchi, K Katori, H Koura, H Kudo, T Ohnishi, A Ozawa, T Suda, K Sueki, F Tokanai, T Yamaguchi, A Yoneda, A Yoshida *J. Phys. Soc. Jpn.* **76** No. 4043201 (2007)
4. K Morita, K Morimoto, D Kaji, T Akiyama, S Goto, H Haba, E Ideguchi, K Katori, H Kikunaga, H Koura, H Kudo, T Ohnishi, A Ozawa, N Sato, T Suda, K Sueki, F Tokanai, T Yamaguchi, A Yoneda, A Yoshida *J. Phys. Soc. Jpn.* **76** 4045001 (2007)
5. Yu Oganessian *J. Phys. G* **34** R165 (2007)
6. Yu Ts Oganessian, V K Utyonkov, Yu V Lobanov, F Sh Abdullin, A N Polyakov, R N Sagaidak, I V Shirokovsky, Yu S Tsyganov, A A Voinov, G G Gulbekian, S L Bogomolov, B N Gikal, A N Mezentsev, S Iliev, V G Subbotin, A M Sukhov, K Subotic, V I Zagrebaev, G K Vostokin, M G Itkis, K J Moody, J B Patin, D A Shaughnessy, M A Stoyer, N J Stoyer, P A Wilk, J M Kenneally, J H Landrum, J F Wild, R W Lougheed *Phys. Rev. C* **74** 044602 (2006)
7. E Haseltine http://discovermagazine com/2002/feb/cover
8. C E Rolfs, W S Rodney, in *Cauldrons in the Cosmos* (Chicago: University of Chicago Press, 1988) p. 469
9. O B Tarasov, T Baumann, A M Amthor, D Bazin, C M Folden III, A Gade, T N Ginter, M Hausmann, M Matoš, D J Morrissey, A Nettleton, M Portillo, A Schiller, B M Sherrill, A Stolz, M Thoennessen *Phys. Rev. C* **75** 064613 (2007)
10. T Baumann, A M Amthor, D Bazin, B A Brown, C M Folden III, A Gade, T N Ginter, M Hausmann, M Matoš, D J Morrissey, M Portillo, A Schiller, B M Sherrill, A Stolz, O B Tarasov, M Thoennessen *Nature (London)* **449** 1022 (2007)
11. K A Gridnev, D K Gridnev, V G Kartavenko, V E Mitroshin, V N Tarasov, D V Tarasov, W Greiner *Int. J. Mod. Phys. E* **15** 673 (2006)
12. V Zagrebaev, W Greiner *Phys. Rev. C* **78** 034610 (2008)
13. V Zagrebaev, W Greiner *Phys. Rev. Lett.* **101** 122701 (2008)
14. K Rutz, M Bender, T Bürvenich, T Schilling, P-G Reinhard, J A Maruhn, W Greiner *Phys. Rev. C* **56** 238 (1997)
15. T Bürvenich, M Bender, J A Maruhn, P-G Reinhard *Phys. Rev. C* **69** 014307 (2004)
16. J Maruhn, W Greiner *Z. Phys.* **251** 431 (1972)
17. M G Itkis, J Äystö, S Beghini, A A Bogachev, L Corradi, O Dorvaux, A Gadea, G Giardina, F Hanappe, I M Itkis, M Jandel, J Kliman, S V Khlebnikov, G N Kniajeva, N A Kondratiev, E M Kozulin, L Krupa, A Latina, T Materna, G Montagnoli, Yu Ts Oganessian, I V Pokrovskya, E V Prokhorova, N Rowley, V A Rubchenya, A Ya Rusanov, R N Sagaidak, F Scarlassara, A M Stefanini, L Stuttge, S Szilner, M Trotta, W H Trzaska, D N Vakhtin, A M Vinodkumar, V M Voskressenski, V I Zagrebaev *Nucl. Phys. A* **734** 136 (2004)
18. V Zagrebaev, W Greiner *Int. J. Mod. Phys. E* **17** 2199 (2008)
19. NRV: Low Energy Nuclear Knowledge Base; http://nrv.jinr.ru/nrv
20. P Möller, J R Nix, W D Myers, W J Swiatecki *At. Data Nucl. Data Tables* **59** 185 (1995)

21. V I Zagrebaev, Y Aritomo, M G Itkis, Yu Ts Oganessian, M Ohta *Phys. Rev. C* **65** 014607 (2002)
22. V I Zagrebaev *Phys. Rev. C* **64** 034606 (2001)
23. R S Naik, W Loveland, P H Sprunger, A M Vinodkumar, D Peterson, C L Jiang, S Zhu, X Tang, E F Moore, P Chowdhury *Phys. Rev. C* **76** 054604 (2007)
24. V Zagrebaev, W Greiner *J. Phys. G* **31** 825 (2005)
25. V Zagrebaev, W Greiner *J. Phys. G* **34** 1 (2007)
26. V I Zagrebaev, A V Karpov, Ya Aritomo, M A Naumenko, W Grainer *Phys. Part. Nucl.* **38** 469 (2007)
27. V I Zagrebaev *AIP Conf. Proc.* **704** 31 (2004)
28. V I Zagrebaev *Nucl. Phys. A* **734** 164 (2004)
29. R Bass, in *Nuclear Reactions with Heavy Ions* (Berlin: Springer, 1980) p. 326
30. A V Eremin, V I Chepigin, M G Itkis, A P Kabachenko, S P Korotkov, O N Malyshev, Yu Ts Oganesyan, A G Popeko, I Roháč, R N Sagaidak, M L Chelnokov, V A Gorshkov, A Yu Lavrent'ev, Z Khofmann, G Müntsenberg, M Vesel'ski, Sh Sharo, K Morita, N Ivasa, S I Mul'gin, S V Zhdanov *JINR Rapid Commun.* (6) 21 (1998)
31. Yu Ts Oganessian, V K Utyonkov, Yu V Lobanov, F Sh Abdullin, A N Polyakov, I V Shirokovsky, Yu S Tsyganov, G G Gulbekian, S L Bogomolov, A N Mezentsev, S Iliev, V G Subbotin, A M Sukhov, A A Voinov, G V Buklanov, K Subotic, V I Zagrebaev, M G Itkis, J B Patin, K J Moody, J F Wild, M A Stoyer, N J Stoyer, D A Shaughnessy, J M Kenneally, R W Lougheed *Phys. Rev. C* **69** 021601 (2004)
32. Yu Ts Oganessian, V K Utyonkov, Yu V Lobanov, F Sh Abdullin, A N Polyakov, I V Shirokovsky, Yu S Tsyganov, G G Gulbekian, S L Bogomolov, B N Gikal, A N Mezentsev, S Iliev, V G Subbotin, A M Sukhov, A A Voinov, G V Buklanov, K Subotic, V I Zagrebaev, M G Itkis, J B Patin, K J Moody, J F Wild, M A Stoyer, N J Stoyer, D A Shaughnessy, J M Kenneally, P A Wilk, R W Lougheed, R I Il'kaev, S P Vesnovskii *Phys. Rev. C* **70** 064609 (2004)
33. Yu Ts Oganessian, V K Utyonkov, Yu V Lobanov, F Sh Abdullin, A N Polyakov, R N Sagaidak, I V Shirokovsky, Yu S Tsyganov, A A Voinov, G G Gulbekian, S L Bogomolov, B N Gikal, A N Mezentsev, V G Subbotin, A M Sukhov, K Subotic, V I Zagrebaev, G K Vostokin, M G Itkis, R A Henderson, J M Kenneally, J H Landrum, K J Moody, D A Shaughnessy, M A Stoyer, N J Stoyer, P A Wilk *Phys. Rev. C* **76** 011601 (2007)
34. K-H Schmidt, W Morawek *Rep. Prog. Phys.* **54** 949 (1991)
35. Yu Ts Oganessian *Phys. At. Nucl.* **69** 932 (2006)
36. V I Zagrebaev, W Greiner *Nucl. Phys. A* **787** C363 (2007)
37. K Siwek-Wilczyńska, I Skwira-Chalot, J Wilczynski *Int. J. Mod. Phys. E* **16** 483 (2007)
38. Yu Ts Oganessian, S N Dmitriev, A V Yeremin, N V Aksenov, G A Bozhikov, V I Chepigin, M L Chelnokov, V Ya Lebedev, O N Malyshev, O V Petrushkin, S V Shishkin, A I Svirikhin, E E Tereshatov, G K Vostokin *Phys. Rev. C* **79** 024608 (2009)
39. W J Światecki, K Siwek-Wilczyńska, J Wilczyński *Phys. Rev. C* **71** 014602 (2005)
40. V I Zagrebaev *Phys. Rev. C* **67** 061601 (2003)
41. V I Zagrebaev, V V Samarin, W Greiner *Phys. Rev. C* **75** 035809 (2007)
42. R J Silva, P F Dittner, M L Mallory, O L Keller, K Eskola, P Eskola, M Nurmia, A Ghiorso *Nucl. Phys. A* **216** 97 (1973)
43. R Dressler, Ph.D. Thesis, University of Bern, Bern, 1999
44. Y Nagame, M Asai, H Haba, S Goto, K Tsukada, I Nishinaka, K Nishio, S Ichikawa, A Toyoshima, K Akiyama, H Nakahara, M Sakama, M Schädel, J V Kratz, H W Gäggeler, A Tmrler *J. Nucl. Rad. Sci.* **3** (1) 85 (2002)
45. W Nörenberg *Phys. Lett. B* **52** 289 (1974)
46. L G Moretto, J S Sventek *Phys. Lett. B* **58** 26(1975)
47. P Frlbrich, S Y Xu *Nucl. Phys. A* **477** 143 (1988)
48. E Vigezzi, A Winther *Ann. Phys. (N.Y.)* **192** 432 (1989)
49. V I Zagrebaev *Ann. Phys. (N.Y.)* **197** 33 (1990)
50. A Winther *Nucl. Phys. A* **594** 203 (1995)
51. K T Davies, A J Sierk, J R Nix *Phys. Rev. C* **13** 2385 (1976)
52. V Zagrebaev, W Greiner *J. Phys. G* **35** 125103 (2008)
53. R L Hahn, P F Dittner, K S Toth, O L Keller *Phys. Rev. C* **10** 1889 (1974)
54. D Lee, H von Gunten, B Jacak, M Nurmia, Y Liu, C Luo, G T Seaborg, D C Hoffman *Phys. Rev. C* **25** 286 (1982)
55. E K Hulet, R W Lougheed, J F Wild, J H Landrum, P C Stevenson, A Ghiorso, J M Nitschke, R J Otto, D J Morrissey, P A Baisden, B F Gavin, D Lee, R J Silva, M M Fowler, G T Seaborg *Phys. Rev. Lett.* **39** 385 (1977)
56. A Türler, H R von Gunten, J D Leyba, D C Hoffman, D M Lee, K E Gregorich, D A Bennett, R M Chasteler, C M Gannett, H L Hall, R A Henderson, M J Nurmia *Phys. Rev. C* **46** 1364 (1992)
57. K J Moody, D Lee, R B Welch, K E Gregorich, G T Seaborg, R W Lougheed, E K Hulet *Phys. Rev. C* **33** 1315 (1986)
58. R B Welch, K J Moody, K E Gregorich, D Lee, G T Seaborg *Phys. Rev. C* **35** 204 (1987)
59. M Schädel, J V Kratz, H Ahrens, W Brüchle, G Franz, H Gäggeler, I Warnecke, G Wirth, G Herrmann, N Trautmann, M Weis *Phys. Rev. Lett.* **41** 469 (1978)
60. M Schädel, W Brüchle, H Gäggeler, J V Kratz, K Sümmerer, G Wirth, G Herrmann, R Stakemann, G Tittel, N Trautmann, J M Nitschke, E K Hulet, R W Lougheed, R L Hahn, R L Ferguson *Phys. Rev. Lett.* **48** 852 (1982)
61. W Mayer, G Beier, J Friese, W Henning, P Kienle, H J Körner, W A Mayer, L Müller, G Rosner, W Wagner *Phys. Lett. B* **152** 162 (1985)
62. V I Zagrebaev, Yu Ts Oganessian, M G Itkis, W Greiner *Phys. Rev. C* **73** 031602 (2006)
63. V Zagrebaev, W Greiner *J. Phys. G* **34** 2265 (2007)
64. J Reinhardt, U Müller, B Müller, W Greiner *Z. Phys. A* **303** 173 (1981)
65. *Quantum Electrodynamics of Strong Fields* (Ed. W Greiner) (New York, London: Plenum, 1983)
66. W Greiner, B Müller, J Rafelski *Quantum Electrodynamics of Strong Fields* (2nd Ed) (Berlin, New York: Springer, 1985)
67. B Fricke, W Greiner *Phys. Lett. B* **30** 317 (1969)
68. B Fricke, W Greiner, J T Waber *Theor. Chim. Acta* **21** 235 (1971)
69. B Fricke, W Greiner *Inseln überschwerer Elemente — die Erweiterung des Periodischen Systems*; Lecture of W Greiner at the Award Ceremony 'Jugend Forscht' at Farbwerke Hoechst AG, Frankfurt, 1972
70. R Eichler, N V Aksenov, A V Belozerov, G A Bozhikov, V I Chepigin, S N Dmitriev, R Dressler, H W Gäggeler, V A Gorshkov, F Haenssler, M G Itkis, A Laube, V Ya Lebedev, O N Malyshev, Yu Ts Oganessian, O V Petrushkin, D Piguet, P Rasmussen, S V Shishkin, A V Shutov, A I Svirikhin, E E Tereshatov, G K Vostokin, M Wegrzecki, A V Yeremin *Nature (London)* **447** 72 (2007)